Werk

Jahr: 1984
Kollektion: fid.geo
Signatur: 8 Z NAT 2148:54
Digitalisiert: Niedersächsische Staats- und Universitätsbibliothek Göttingen
Werk Id: PPN1015067948_0054
PURL: http://resolver.sub.uni-goettingen.de/purl?PPN1015067948_0054

LOG Id: LOG_0011
LOG Titel: Plate dynamics and isostasy in a dynamic system
LOG Typ: article

Übergeordnetes Werk

Werk Id: PPN1015067948
PURL: http://resolver.sub.uni-goettingen.de/purl?PPN1015067948
OPAC: http://opac.sub.uni-goettingen.de/DB=1/PPN?PPN=1015067948

Contact

Niedersächsische Staats- und Universitätsbibliothek Göttingen
Georg-August-Universität Göttingen
Platz der Göttinger Sieben 1
37073 Göttingen
Germany
Email: gdz@sub.uni-goettingen.de

J Geophys (1983) 54:1-19

Journal of Geophysics

Plate dynamics and isostasy in a dynamic system

C.B. Officer and C.L. Drake

Earth Sciences Department, Dartmouth College, Hanover, N.H. 03755, USA

Abstract. A quantitative description of plate dynamics and related upper mantle effects is given. The principal driving force for the upper mantle convection is the longitudinal density gradient in the upper mantle between the spreading ridge and subduction zone. The effects of plate forces, asthenospheric-lithospheric coupling, lithospheric density changes, and viscosity variations as a function of depth are considered and included in the derivations. The results are applied to a description of the observed plate velocities, plate velocity variations as a function of plate geometry, asymmetric seafloor spreading, spreading ridge migration, global gravity anomalies, ocean floor relief, and asymmetric variations in ocean floor relief.

Key words: Plate tectonics – Mantle convection – Isostasy

Preface

Introduction

The purpose of this paper is to present a quantitative description of plate dynamics and associated effects of isostasy in a dynamic system. The principal driving force for the upper mantle convection that is proposed is that related to the longitudinal density gradient in the upper mantle between the spreading ridge and the subduction zone. Although such longitudinal density gradient circulation is a familiar feature of other geophysical fluid dynamic problems, it has only recently been emphasized by Rabinowicz et al. (1980) and Hewitt et al. (1980) in their theoretical investigations and by Irvine (1979), Froidevaux and Nataf (1981), Nataf et al. (1981), and Carrigan (1982) in their experimental investigations as an explanation for plate tectonics.

Our description is restricted solely to plate dynamics and related upper mantle effects. It does not cover possible whole mantle convection. It is also restricted to the drifting phase of plate tectonics. It is not intended to apply to the beginning, or rifting, phase of plate tectonics where the description originally given by Pekeris (1935) may be applicable.

In this description the plates are carried along as inertial elements by the convective motion in the upper mantle between the spreading ridge and the subduction zone. The effects of plate forces, asthenospheric-lithospheric coupling, and lithospheric density changes are also considered and included in the quantitative description as well as possible depth variations of viscosity in the upper mantle.

The results are applied to a description of the observed plate velocities, plate velocity variations as a function of plate geometry, asymmetric seafloor spreading, spreading ridge migration, global gravity anomalies, ocean floor relief, and asymmetric variations in ocean floor relief.

Defining equations and model parameters

The Navier-Stokes motion equation and the appropriate continuity equations are used with the usual reductions to upper mantle motion as delineated, for example, by McKenzie (1968) and Richter (1973). Only analytic solutions are given here. We ascribe to the premise stated by Richter (1973) that unless simple models are first understood, complex cases will not be interpretable in terms of the contributions to the overall flow that each possible source of motion provides. It is essential to have an adequate understanding and explanation of the various plate dynamic observables in terms of simple theory before the requisite numerical computational procedures can appropriately be made.

Again following McKenzie (1968) and Richter (1973) as well as others, the earth model and parameters chosen are summarized in Table 1. A nominal lithospheric plate thickness of $d = 100$ km, a depth extent for the upper mantle convection of $h = 600$ km with a viscosity of $\nu = 3 \times 10^{21}$ cm^2 s^{-1}, and a nominal upper mantle density of $\rho_0 = 3.5$ gm cm^{-3} are chosen. The depth extent of the upper mantle convection is taken to coincide both with the depth extent of the subducted slab in the upper mantle and a corresponding depth extent of the density anomaly associated with the spreading ridge region and with the depth extent of the low viscosity region of the upper mantle. A nominal, average, density deficit of $\sigma = 0.02$ gm cm^{-3} over the depth extent, h, is taken for the spreading ridge region and a corresponding density excess of the same amount for the subducted slab. It is appreciated that there are differences of opinion as to the depth variations of viscosity in the upper mantle as discussed by McKenzie (1966), McConnell (1968), Cathles (1975), Peltier and

Table 1. Values of mantle parameters used in calculations

$\nu = 3 \times 10^{21}\ \mathrm{cm^2\,s^{-1}}$	$g = 10^3\ \mathrm{cm\,s^{-2}}$
$\sigma = 0.02\ \mathrm{gm\,cm^{-3}}$	$h = 600\ \mathrm{km}$
$\rho_0 = 3.5\ \mathrm{gm\,cm^{-3}}$	$d = 100\ \mathrm{km}$

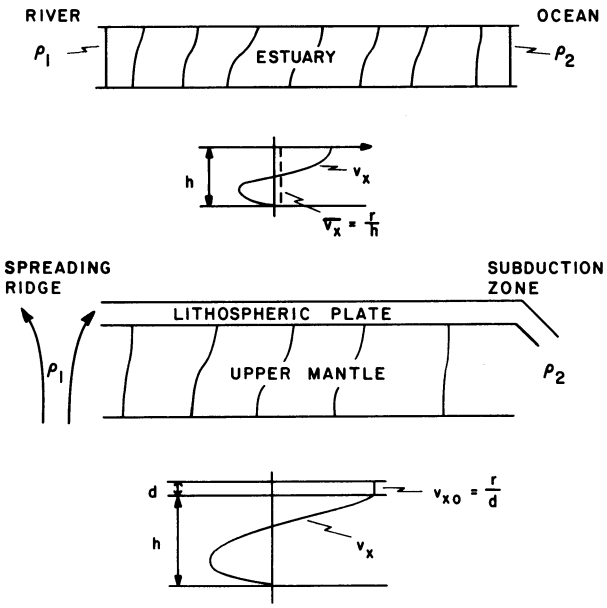

Fig. 1. a Density profiles and velocity distribution in central portion of flow regime for longitudinal density gradient circulation in an estuary. **b** Corresponding profiles and velocity distribution for upper mantle circulation

Andrews (1976) and Sammis et al. (1977) as well as others, and this is a critical parameter in the description of any upper mantle convection. We consider the effects of such extended depth variations in viscosity retaining the same depth extent for the driving forces.

Longitudinal density gradient circulation

At the outset it is appropriate to consider some of the characteristics of longitudinal density gradient, or gravitational, circulation. A particular example which has relevance to the proposed upper mantle circulation is that of gravitational circulation in an estuary. The longitudinal density gradient is related to the density difference from the freshwater river end of the estuary to the more saline waters at the ocean end of the estuary, a contrast with a characteristic value of $0.02\ \mathrm{gm\,cm^{-3}}$. The corollary to the upper mantle is the spreading ridge region, maintained at a density deficit as compared with average upper mantle conditions because of its higher temperature related to the continuing plate forming process, and the subduction zone, maintained at a corresponding density excess because of the continued subduction of the cooler slab into the upper mantle. These relations are shown schematically in Fig. 1. The length of an estuary has a characteristic value of 10 km or more and a depth of 10 m, or an aspect ratio of 1000:1; for the upper mantle the aspect ratio is of the order of 10:1.

The theoretical description of gravitational circulation in estuaries has been given by Rattray and Hansen (1962) and Hansen and Rattray (1965) using similarity solution procedures and a simplified description applicable to the central regime of an estuary where the longitudinal density gradient and surface slope may be considered constant by Officer (1976). A more detailed numerical model description of the same process has been given by Festa and Hansen (1976). The characteristic circulation velocity profile for the central regime of an estuary and also for the upper mantle have been included in Fig. 1. With the much lower eddy viscosity coefficient values for estuarine waters, the circulation flows have characteristic values of $10\ \mathrm{cm\,s^{-1}}$, down-estuary in the upper part of the water column and up-estuary in the lower part of the water column.

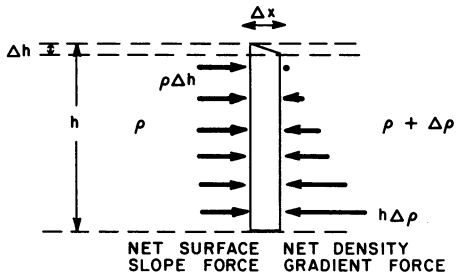

Fig. 2. Diagram of net horizontal forces across a vertical slab for longitudinal density gradient circulation

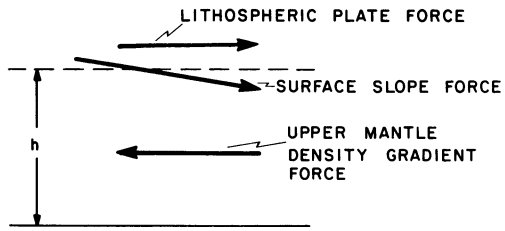

Fig. 3. Driving forces for upper mantle convection and lithospheric plate coupling

The physics of gravitational circulation can be understood from a consideration of the horizontal force balance across a vertical slab normal to the flow, as shown in Fig. 2. The driving forces for the circulation are the longitudinal surface slope force, acting in a direction from the river (spreading ridge) toward the ocean (subduction zone) and the longitudinal density gradient force, acting in the opposite direction. The surface slope force is constant as a function of depth, and the density gradient force increases essentially linearly as a function of depth. The net effect, then, is that the surface slope force will be dominant in the upper portion of the water column (upper mantle), producing a net circulation flow to the right in the diagram, and that the density gradient force will be dominant in the lower portion, producing a net circulation flow to the left in the diagram within the constraints of the depth averaged continuity relation.

For both cases there can be an additional force at the upper surface, as shown in Fig. 3. For an estuary this is the wind stress and for the upper mantle it is the net lithospheric plate force. If this force is in the direction of the surface slope, it will increase the circulation velocity near the upper surface and correspondingly the

resultant lithospheric plate velocity. Without such a surface drive, or drag, force, the lithospheric plate will move as a passive element with the upper mantle convection. With the addition of a plate force, the plate velocity will be increased or decreased accordingly as the force is a net drive or drag.

Upper mantle variations

An essential feature necessary for gravitational circulation is the continued maintenance of different densities at each end of the circulation regime. This is, indeed, the case for the upper mantle at the spreading ridge and the subduction zone. For an assumed average temperature excess of 140 °C over a depth extent of 600 km at the spreading ridge, a density deficit of 0.02 gm cm^{-3} would result. From Minear and Toksöz (1970) and Toksöz (1975) as well as others, an average temperature deficit and corresponding density excess of the same magnitude is anticipated at the subduction zone. We have chosen an average density anomaly of $\sigma = 0.02$ gm cm^{-3} at each end of the convection cell and consider this value to be reasonable and, if anything, on the low side. Ringwood (1982), for example, discusses average density anomalies in excess of this value for the subducted slab including the combined effects of temperature and phase changes.

As in most hypotheses of plate dynamics and upper mantle convection, the ultimate cause for the driving forces is presumed to be heat. Implicit in the upper mantle gravitational circulation discussed herein is the assumption that the major heat related effects are restricted to the spreading ridge and subduction zone regimes. This assumption is confirmed, at least in part, by the results of Sclater et al. (1981) that more than 60% of the heat loss from the earth results from the creation of oceanic plates.

Further, for gravitational circulation in the upper mantle there will be a resultant longitudinal density change increasing from the spreading ridge to the subduction zone for a given plate. As discussed by Jordan (1975, 1979) as well as others, such upper mantle changes can be inferred from seismological observations. Jordan (1979) shows longer *ScS* travel times from a depth of 700 km to the surface of 2 s under young oceanic crust as compared with old oceanic crust. This change is in the correct direction and order of magnitude as would be anticipated for lower average density, upper mantle material near a spreading ridge as contrasted with higher density, upper mantle material near a subduction zone with a total average density change of around $2\sigma = 0.04$ gm cm^{-3}.

Plate dynamics

Linear approximation

The linear approximation assumes that the longitudinal dimension, l, of the upper mantle convection is large with respect to the vertical dimension, h. The interest, here, is in examining the central region of the convection cell where it is reasonable to assume that the longitudinal variation in density, ρ, and the upper and lower surfaces, ξ_s and ξ_b, of the convection cell are linear with respect to the horizontal dimension, x, over limited distances. The geometry is shown in Fig. 4. Following Officer (1976) the motion equation reduces to

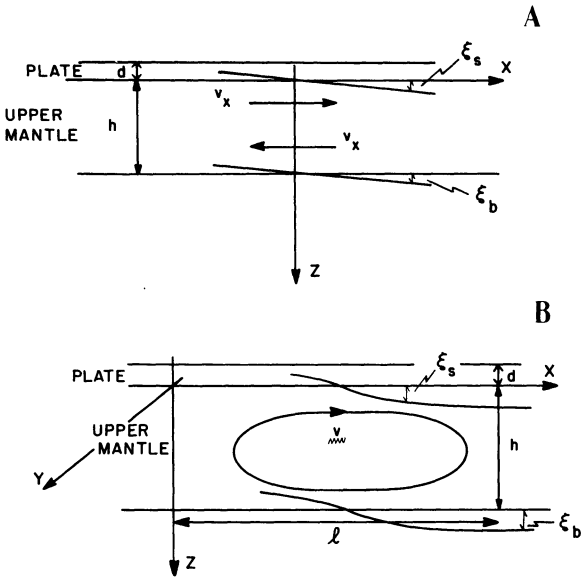

Fig. 4a+b. **a** Geometry for linear approximation. **b** Geometry for two dimensional flow

$$\frac{\partial p}{\partial x} = \rho_0 \nu \frac{\partial^2 v_x}{\partial z^2} \tag{1}$$

under steady state conditions and with the assumption that the upper mantle motion is sufficiently slow that the inertial terms may be neglected with respect to the viscous and buoyancy terms. In this equation p is the pressure, v_x the horizontal velocity, ν the upper mantle kinematic viscosity coefficient, and ρ_0 an upper mantle reference density.

For the definition of the convective cell under the linear approximation there are two boundary conditions at the upper surface of the convection cell, one boundary condition at the lower surface, and a continuity condition. At the outset we shall take a condition of normal stress balance at the upper surface of the convection cell, i.e., no normal stress contribution from mass variations in the overlying lithosphere. Also, in this first instance we shall take a condition in which there are no plate drive or drag forces, i.e., inertial plate motion with no tangential stress coupling to the mantle, or $\partial v_x/\partial z = 0$, $z = 0$. At the lower surface we shall take a condition of no motion, or $v_x = 0$, $z = h$. For the continuity relation we shall take a condition that the mantle motion is self contained, or $\int_0^h v_x \, dz = 0$.

From the first boundary condition at the upper surface we have

$$p = \rho g (z - \xi_s) + p_0 \tag{2}$$

where p_0 is a reference, constant normal stress or in this case of a linear approximation, constant pressure. We, then, have for the longitudinal pressure gradient

$$\frac{\partial p}{\partial x} = g \int_0^z \frac{\partial \rho}{\partial x} dz - \rho_0 g \frac{\partial \xi_s}{\partial x}$$
$$= g \lambda z - \rho_0 g i_s \tag{3}$$

where we have ignored the second order term in $\xi_s(\partial\rho/\partial x)$ and where $i_s=\partial\xi_s/\partial x$ is the upper surface slope and $\lambda=\partial\rho/\partial x$ the longitudinal density gradient, taken in this initial example to be independent of z. Substituting Eq. (3) into Eq. (1), we have a simple ordinary differential equation. The second boundary condition at the upper surface and the boundary condition at the lower surface determine the two integration constants and the continuity condition provides the relation between the surface slope, i_s, and the longitudinal density gradient, λ, giving

$$v_x=\frac{1}{48}\frac{g\lambda h^3}{\rho_0 v}(1-9n^2+8n^3),\ i_s=\frac{3}{8}\frac{\lambda h}{\rho_0} \tag{4}$$

where $n=z/h$ is the scaled depth. It is to be noted that the magnitude of v_x is proportional to $\lambda h^3/v$. The horizontal velocity, v_{x0}, at the upper surface of the convection cell is then

$$v_{x0}=\frac{1}{48}\frac{g\lambda h^3}{\rho_0 v}. \tag{5}$$

As another example we take the case for which there is infinite plate resistance to the upper mantle motion, changing the second boundary at the upper surface to $v_x=0$, $z=0$. The corresponding solution is

$$v_x=\frac{1}{48}\frac{g\lambda h^3}{\rho_0 v}(4n-12n^2+8n^3),\ i_s=\frac{1}{2}\frac{\lambda h}{\rho_0}. \tag{6}$$

The tangential stress, τ_{zx0}, at $z=0$ is then a maximum, given by

$$\tau_{zx0}=\rho_0 v\frac{\partial v_x}{\partial z}=\frac{1}{12}g\lambda h^2 \tag{7}$$

As two further examples we take extreme cases for which there is a z dependence in the λ term such that $\partial\rho/\partial x=\lambda_0[1-(z/h)]$ and $\partial\rho/\partial x=\lambda_0(z/h)$. The solutions for v_x corresponding to relation (4), are respectively,

$$v_x=\frac{1}{240}\frac{g\lambda_0 h^3}{\rho_0 v}(3-33n^2+40n^3-10n^4),\ i_s=\frac{11}{40}\frac{\lambda_0 h}{\rho_0} \tag{8}$$

$$v_x=\frac{1}{120}\frac{g\lambda_0 h^3}{\rho_0 v}(1-6n^2+5n^4),\qquad i_s=\frac{1}{10}\frac{\lambda_0 h}{\rho_0} \tag{9}$$

It is to be noted that the horizontal velocity, v_{x0}, at the surface is reduced to 0.6 and 0.4 the value given by relation (4) for the two cases, as might be expected for the corresponding reduction in the longitudinal density gradient forcing term.

The first boundary condition at the upper surface of the convection cell requires additional attention. For a lithosphere in isostatic equilibrium the combined vertical stresses of the mass per unit column and the lithospheric strength stresses related to regional isostatic equilibrium will be the same everywhere at the depth of the upper surface of the convection cell. The normal stress condition of Eq. (2) remains the same. It is appreciated that for time periods comparable to lithospheric adjustment times, such as that for the Fennoscandia uplift following deglaciation, there will be a lithospheric loading contribution to the upper mantle motion.

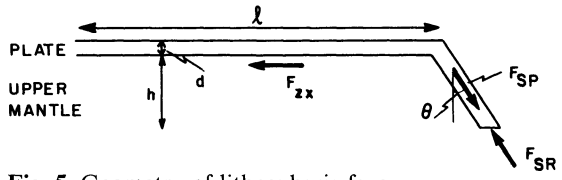

Fig. 5. Geometry of lithospheric forces

The continuity relation also requires additional attention. We have assumed that the upper mantle convection cell motion is self contained, or that $\int_0^h v_x dz=0$. We could choose an alternative continuity relation that both the plate formation and destruction are confined to the upper mantle so that the continuity relation would, then, $v_{x0}d+\int_0^h v_x dz=0$, where d is the plate thickness. The results corresponding to Eqs. (4) and (5) are

$$v_x=\frac{1}{48}\frac{g\lambda h^3}{\rho_0 v}\left[\frac{1-9n^2+8n^3-12\delta(n^2-n^3)}{1+1.5\delta}\right],$$

$$i_s=\frac{3+4\delta}{8+12\delta}\frac{\lambda h}{\rho_0} \tag{10}$$

and

$$v_{x0}=\frac{1}{48}\frac{g\lambda h^3}{\rho_0 v}\left[\frac{1}{1+1.5\delta}\right] \tag{11}$$

where $\delta=d/h$ is the ratio of the lithospheric plate thickness to the depth extent of the upper mantle convection. For values of $d=100$ km and $h=600$ km, as given in Table 1, v_{x0} will be reduced by 20% over the value given by Eq. (5). The inclusion of this continuity condition has a small effect on the circulation, reducing the circulation velocities at all depths. The dominant effect is still that of the longitudinal density gradient.

Asthenospheric-lithospheric coupling

To this point we have considered the lithospheric plate as a passive element, moving along with the inertial velocity, v_{x0}, of the upper mantle convection as driven by the longitudinal density gradient. We must also consider the active effects of the drive and drag forces on the lithospheric plate itself and the coupling of these forces with the upper mantle convection.

From Forsyth and Uyeda (1975), Chapple and Tullis (1977) and Backus et al. (1981) the principal plate forces are the negative buoyancy drive force of the descending slab, F_{SP}, in the subduction zone and the corresponding viscous resistance, F_{SR}, to its descent, as shown in Fig. 5. We have included a mantle drag force, F_{zx}, to the force balance. The slab pull force is given simply by

$$F_{SP}=g\sigma V\sin\theta=g\sigma dh \tag{12}$$

where V is the volume of the descending slab and σ the average density contrast and where, for convenience, we have taken the depth of descent to correspond with that for the upper mantle convection, h. The slab resistance force is taken to be proportional to the plate ve-

locity, v_{x0}, or

$$F_{SR}=Rv_{x0} \tag{13}$$

where R is a resistance coefficient. For unaccelerated plate motion the plate forces must balance, giving

$$F_{SP}-F_{zx}-Rv_{x0}=0. \tag{14}$$

The tangential stress condition at the upper surface of the convection cell, then, becomes

$$\tau_{zx0}=\rho_0 \nu \frac{\partial v_x}{\partial z}=-f_{zx}=-\frac{F_{zx}}{l}=-\frac{F_{SP}-Rv_{x0}}{l} \tag{15}$$

where l is the plate length. From Officer (1976) the solution, corresponding to Eqs. (4) and (5), is

$$v_x=\frac{1}{48}\frac{g\lambda h^3}{\rho_0 \nu}(1-9n^2+8n^3)+\frac{1}{4}\frac{hf_{zx}}{\rho_0 \nu}(1-4n+3n^2),$$
$$i_s=\frac{3}{8}\frac{\lambda h}{\rho_0}-\frac{3}{2}\frac{f_{zx}}{\rho_0 g h} \tag{16}$$

and

$$v_{x0}=\frac{1}{6}\frac{g\sigma h^3+6g\sigma d h^2}{4\rho_0 \nu l+hR} \tag{17}$$

where in Eq. (17) we have substituted for τ_{zx0} from Eqs. (15) and (12) and where we have also made the substitution for the linear approximation that $\lambda=\partial\rho/\partial x=2\sigma/l$ where σ is the average density deficit at the spreading ridge and the corresponding density excess at the subduction zone over the depth interval of the upper mantle convection.

It is instructive to examine the values for v_{x0} in certain limiting cases for the plate forces. For $R=\infty$, $v_{x0}=0$ and the tangential stress on the lithospheric plate from the underlying mantle convection is given by Eq. (7). For $F_{SP}=F_{SR}$, the preferred condition of Forsyth and Uyeda (1975), the plate velocity is given by

$$v_{x0}=\frac{1}{24}\frac{g\sigma h^3}{\rho_0 \nu l} \tag{18}$$

the same as that of Eq. (5). For no slab resistance, $R=0$ and

$$v_{x0}=\frac{1}{24}\frac{g\sigma h^3+6g\sigma d h^2}{\rho_0 \nu l}. \tag{19}$$

In the model used in the following sections, $d=100$ km and $h=600$ km so that the first and second terms in the numerator of Eq. (19) are equal. The plate velocity under these conditions is twice that of no net lithospheric drive or drag force. These various velocity relations are shown graphically in Fig. 6.

Richter (1973, 1977) and Richter and McKenzie (1978) have invoked an alternative driving mechanism for the upper mantle convection. They have considered only the net driving stress, f_{zx}, with no longitudinal density gradient circulation in the mantle itself. In other words, they consider the upper mantle convection as a passive element in the asthenospheric-lithospheric coupling and that the upper mantle convection is a resultant effect solely of the net plate forces. Their formulation is an attractive alternative; for as shown above in Eq. (19), the plate velocity, v_{x0}, can have comparable contributions from both the upper mantle, longitudinal density gradient effects and the lithospheric plate, net driving force effects.

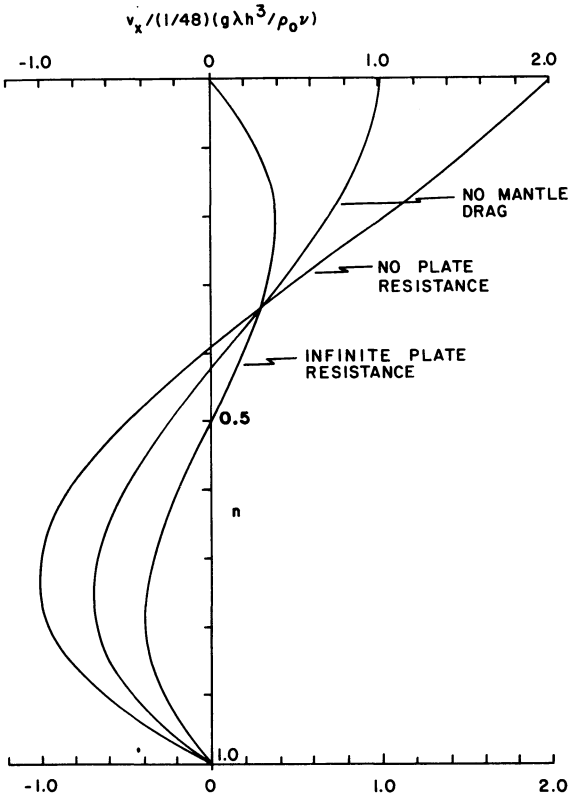

Fig. 6. Graph of scaled convection current velocity, $v_x/(1/48)(g\lambda h^3/\rho_0 \nu)$, versus scaled depth, $n=z/h$, for various lithospheric plate conditions

It is instructive to formulate their problem in the same terms as given above and to compare the results obtained therewith. They considered a continuity relation in the same form as that used for Eqs. (10) and (11). From Officer (1976) the complete solution including both the longitudinal density gradient and plate stress contributions is

$$v_x=\frac{1}{48}\frac{g\lambda h^3}{\rho_0 \nu}\left[\frac{1-9n^2+8n^3-12\delta(n^2-n^3)}{1+1.5\delta}\right]$$
$$+\frac{1}{4}\frac{hf_{zx}}{\rho_0 \nu}\left[\frac{1-4n+3n^2-6\delta(n-n^2)}{1+1.5\delta}\right],$$
$$i_s=\frac{3+4\delta}{8+12\delta}\frac{\lambda h}{\rho_0}-\frac{3+6\delta}{2+3\delta}\frac{f_{zx}}{\rho_0 g h} \tag{20}$$

and

$$v_{x0}=\frac{1}{48}\frac{g\lambda h^3}{\rho_0 \nu}\left[\frac{1}{1+1.5\delta}\right]+\frac{1}{4}\frac{hf_{zx}}{\rho_0 \nu}\left[\frac{1}{1+1.5\delta}\right]. \tag{21}$$

The second terms in each of these three expressions correspond to the formulation given by Richter and McKenzie (1978).

There is a basic objection to ignoring the first terms in Eqs. (20) and (21). The longitudinal density gradient

contribution is an integral component of the formulation in addition to the plate stress contribution. It is incorrect to ignore it *a priori*. A more pertinent question would be under what conditions are the second terms dominant over the first terms. As we have shown in the discussion of Eqs. (17) to (19), the plate stress contribution can be comparable to the density gradient contribution only under idealized conditions of minimal slab resistance, F_{SR}, for the model chosen. It is to be noted, however, that with decreasing values for the depth extent, h, of the upper mantle convection the plate stress term effects will increase with respect to the density gradient term effects. In order to maintain comparable plate velocities, v_{x0}, this necessarily implies a corresponding decrease in the viscosity of the uppermost mantle, as elaborated by Richter (1977) and Richter and McKenzie (1978).

In addition there are the following three considerations which argue against the dominance of the f_{zx} term over the λ term. First, as delineated by Forsyth and Uyeda (1975) and Backus et al. (1981), the principal plate resistance force is F_{SR} which would argue for the formulation given by Eq. (18) as contrasted with Eq. (19) where $F_{SR}=0$ and F_{zx} is the dominant resistance force. Second, the contribution to the slope, i_s, of the upper surface of the mantle convection from the f_{zx} term is negative to that from the λ contribution. This is understandable since as shown in Fig. 3, both the slope and plate stress forces are in the same direction; and an increase in f_{zx} will have the effect of decreasing i_s to provide the necessary balance with the λ term in the opposite direction in the continuity integral. If there were no longitudinal density gradient effect, i_s would be negative, i.e., a slope of the upper surface down in the direction from the subduction zone toward the spreading ridge. For illustration, let us presume in Eq. (16) that $\lambda=0$ and we wish to have the same value for v_{x0} under the condition of $f_{zx}=0$, or simply $(1/48)(g\lambda h^3/\rho_0 \nu)=(1/4)(hf_{zx}/\rho_0 \nu)$; then, the resultant slope, i_{s2}, will be such that $i_{s2}=-(1/3)i_{s1}$ where $i_{s1}=(3/8)(\lambda h/\rho_0)$. The magnitude of the two slopes are comparable but in opposite directions. As discussed in a following section on ocean floor relief, the oceanic depths for plate ages greater than 70 m.y. continue to increase in the direction from the spreading ridge toward the subduction zone and can be interpreted in terms of the i_{s1} slope term. Third, the formulation without the first terms in Eqs. (20) and (21) would argue that there are no appreciable changes in the upper mantle density. As discussed previously, the available evidence would argue that there are, indeed, longitudinal density changes which are associated with plate geometry.

Our conclusion is that the longitudinal density gradient effects are an essential constituent to the understanding of upper mantle convection and plate motion and that the net stress related to asthenospheric-lithospheric coupling can provide an additional contribution.

Plate velocities and plate geometry

Equation (18) expresses a simple relation between plate velocity and plate geometry, specifically that the plate velocity, v_{x0}, is inversely proportional to the longitudinal extent, l, of the plate. It is of interest to see if this

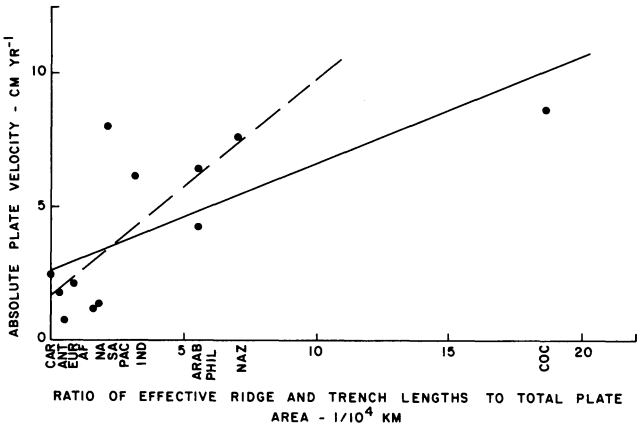

Fig. 7. Graph of absolute plate velocities versus the ratio of sum of effective ridge and trench lengths to total plate area

relation, derived from a linear approximation, is applicable to actual plate geometries and velocities, appreciating that the relation does not include the actual plate geometry and effects between plates.

Considering b_1 and b_2 as the lateral extents of a plate and b'_1 and b'_2 as their effective ridge and trench lengths, the quantity, σ, in Eq. (18) will be scaled to $\sigma' = (b'_1+b'_2)\,\sigma/(b_1+b_2)$. Equation (18) may then be rewritten as

$$v_{x0}=\frac{1}{48}\,\frac{g\sigma h^3}{\rho_0 \nu}\,\frac{b'_1+b'_2}{A} \tag{22}$$

where $A=(b_1+b_2)\,l/2$ is the plate area. Forsyth and Uyeda (1975) have summarized estimates of absolute plate velocities, effective spreading ridge and subduction zone lengths, and total plate areas. Using the values in their Table 1 we obtain the plot shown in Fig. 7. Considering the gross assumption made above and the uncertainties in determining the plotted data, the agreement is quite reasonable and in the right sense. For those plates with low absolute velocities of around 1–2 cm yr^{-1}, the ratio $(b'_1+b'_2)/A$ is small; for those plates with high absolute velocities of around 5–8 cm yr^{-1}, the ratio $(b'_1+b'_2)/A$ is larger.

It is possible to carry the analysis a step further. A value for h can be determined using the estimates for σ, ρ_0 and ν of Table 1. The solid line in Fig. 7 is the linear least square fit to all the data and the dashed line the corresponding fit to the data with the exclusion of the Cocos plate. From Eq. (22), $h=690$ km for the solid line slope and $h=870$ km for the dashed line slope. The analysis procedure is, at best, crude but it is encouraging that it comes out with reasonable values for the parameter, h.

This comparison of plate velocities with plate geometry is neither intended to be definitive in itself nor to exclude correlations with other geometrical parameters. In particular, Gordon et al. (1978) correlate plate velocities with the effective ridge and trench lengths, considering the plate driving forces to be related equally to a ridge push and a slab pull. In our formulation these terms are also included as the effective driving forces for an upper mantle, gravitational circulation in the quantity, $b'_1+b'_2$, of Eq. (22) with the exception that we

have applied b_2' to both adjoining plates. Carlson (1981) has made a similar comparison with the inclusion of a continental drag component. Also, Carlson et al. (1983) have correlated plate velocities with the ages, or thicknesses, of the lithospheric plates at the subduction zones using simple but reasonable expressions for the slab pull, F_{SP}, and slab F_{SR}, forces. As discussed in the previous section, our analysis indicates that these forces can provide an additional and important contribution to the upper mantle, gravitational circulation in determining plate velocities.

Two dimensional approximation

The formulation and solution procedures used here follow along the same lines as those used previously by Allan et al. (1967) and McKenzie (1968). The motion equation, corresponding to Eq. (1), is

$$\rho_0 \nu \nabla^2 \mathbf{v} = \nabla p - \rho \mathbf{g} \tag{23}$$

or in vorticity equation form

$$\nabla^2(\nabla \times \mathbf{v}) = -\frac{1}{\rho_0 \nu} \nabla \rho \times \mathbf{g}. \tag{24}$$

From the continuity equation

$$\nabla \cdot \mathbf{v} = 0 \tag{25}$$

the longitudinal and vertical velocity components may be given in terms of a scalar stream function, ψ, by

$$v_x = -\frac{\partial \psi}{\partial z}, \quad v_z = \frac{\partial \psi}{\partial x} \tag{26}$$

reducing the vorticity equation to

$$\nabla^4 \psi = -\frac{g}{\rho_0 \nu} \frac{\partial \rho}{\partial x}. \tag{27}$$

It is to be noted from Eqs. (24) and (27), as has been pointed out by others, that the important variable determining the upper mantle convective motion is the horizontal density gradient.

In general, the problem resolves to the solution of a set of coupled partial differential equations, Eq. (27) and the thermal and chemical continuity equations with the appropriate nonadvective and advective transfer terms. It is not our intention, here, to attempt to solve this set of coupled equations but rather to assume a reasonable form for the longitudinal density variation, $\partial \rho / \partial x$, in order to be able to determine the principal dependencies for the longitudinal velocity, v_x. For the inner, or near spreading ridge, regime there will be an accelerated horizontal flow and for the outer, or near subduction zone, regime there will be a decelerated horizontal flow with a central regime of unaccelerated flow, as given by the linear approximation solutions of the previous section. Consequently, we have taken as a first approximation that the longitudinal density variation may be represented by its first Fourier component

$$\rho = -\sigma \cos kx + f(z) \tag{28}$$

or

$$\frac{\partial \rho}{\partial x} = k\sigma \sin kx \tag{29}$$

where σ is the average density deficiency in the upper mantle at the spreading ridge and corresponding density excess in the subduction zone and where k is a wavenumber, defined by $k = \pi/l$, with the geometry of Fig. 4.

Upon substituting Eq. (29) into Eq. (27) with the corresponding form for the stream function

$$\psi = \phi(z) \sin kx \tag{30}$$

we obtain

$$\frac{d^4\phi}{dz^4} - 2k^2 \frac{d^2\phi}{dz^2} + k^4 \phi = -\frac{g\sigma k}{\rho_0 \nu} \tag{31}$$

an ordinary differential equation. The four boundary conditions used are $\tau_{zx} = 0$, $v_z = 0$ at $z = 0$ and $v_x = 0$, $v_z = 0$ at $z = h$. The solution for ψ is

$$\psi = -\frac{g\sigma \sin kx}{2\rho_0 \nu k^3} \left[kz \sinh kz + 2(1 - \cosh kz) + \frac{L\, kz \cosh kz - M \sinh kz}{kh - \sinh kh \cosh kh} \right] \tag{32}$$

where

$$L = 1 - 2\cosh kh + \cosh^2 kh$$
$$M = k^2 h^2 - 2\cosh kh + 2\cosh^2 kh - 2kh \sinh kh. \tag{33}$$

The corresponding solution for the longitudinal velocity, v_{x0}, at the upper surface is

$$v_{x0} = \frac{g\sigma}{2\rho_0 \nu k^2} N(\eta) \sin kx \tag{34}$$

where $N(\eta)$ is given by

$$N(\eta) = \frac{2\eta \sinh \eta - \eta^2 - \sinh^2 \eta}{\eta - \sinh \eta \cosh \eta} \tag{35}$$

where $\eta = kh$. For η small, v_{x0} reduces to

$$v_{x0} = \frac{1}{48} \frac{g\sigma k h^3}{\rho_0 \nu} \sin kx \tag{36}$$

which is the same as the value given by Eq. (5), remembering that Eq. (5) refers to the central regime where $\lambda = \partial \rho / \partial x = k\sigma$.

Figure 8 is a plot of the amplitude of v_{x0} from Eq. (34) versus plate length, l, and aspect ratio, l/h, using the parameters of Table 1. The numerical formula for these calculations is

$$v_{x0} = 30.44\, l^2\, N(\eta) \sin kx \tag{37}$$

where l is in 10^3 km and v_{x0} in cm yr^{-1}. For η small, $N(\eta)$ approaches the limiting value $(1/24)\eta^3$. To first figure accuracy in v_{x0}, this corresponds to values of $(l/h) \geqq 2.5$, or to values of $l \geqq 1{,}500$ km. Under these conditions the formula (36) reduces to

$$v_{x0} = 8.49\, l^{-1} \sin kx. \tag{38}$$

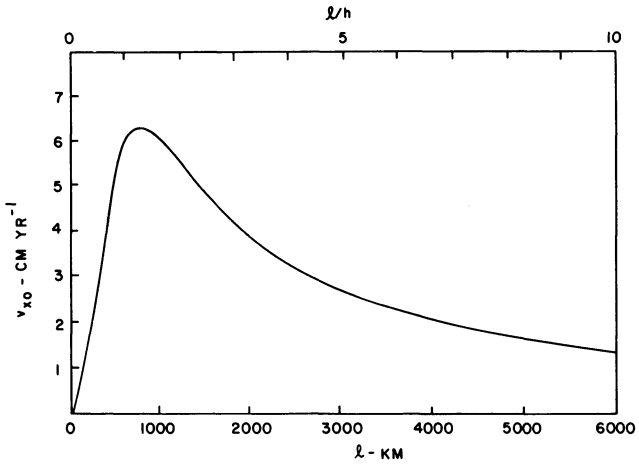

Fig. 8. Graph of amplitude of mantle convection velocity in cm yr^{-1} versus longitudinal extent of convection cell, l, in km

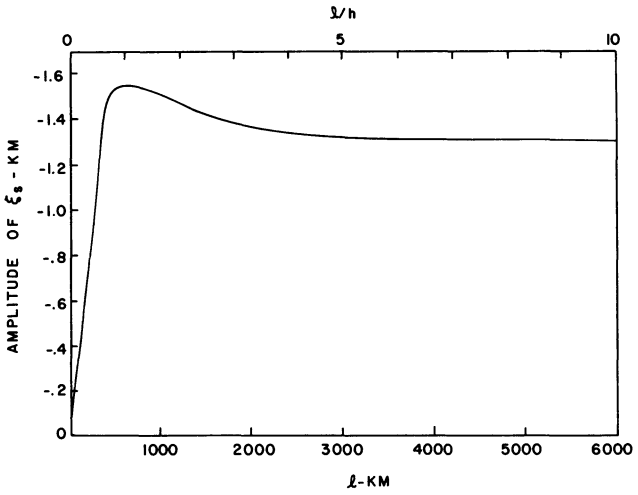

Fig. 9. Graph of amplitude of deformation of upper surface of mantle convecting layer, ξ_s, in km versus longitudinal extent of cell, l, in km

It is to be noted that the calculated velocities are in the observed range of plate velocities and that for the major plates of the earth, v_{x0} would vary inversely as l.

The deformation of the upper surface of the mantle convection cell, $\xi_s = \xi_{0s} \cos kx$, may be obtained from the additional condition that the normal stress related to the convective motion must vanish on this surface, or

$$\left[-p_0 - p' + 2\rho_0 \nu \frac{\partial v_z}{\partial z}\right]_{\xi_s} = 0. \tag{39}$$

The total pressure is given by $p = p_0 + p'$ where $p_0 = \rho_0 g z$ is the hydrostatic pressure and p' is the pressure related to the convective motion. The quantity p' may be obtained from the reduced form of Eq. (24) and the determined value of ψ, giving

$$p' = -\frac{g\sigma}{k}\left[\sinh kz + \frac{L \cosh kz}{kh - \sinh kh \cosh kh}\right] \cos kz. \tag{40}$$

To first order terms, the result for ξ_{0s} is

$$\xi_{0s} = -\frac{\sigma}{\rho_0 k} P(\eta) \tag{41}$$

where

$$P(\eta) = \frac{2\cosh\eta - 2\cosh^2\eta + 2\eta \sinh\eta - \eta^2}{\eta - \sinh\eta \cosh\eta}. \tag{42}$$

For η small, ξ_{0s} reduces to

$$\xi_{0s} = -\frac{3}{8}\frac{\sigma h}{\rho_0} \tag{43}$$

which gives the same slope, i_s, for the central regime as the second part of Eq. (4), remembering as before that $\lambda = \partial\rho/\partial x = k\sigma$ in the central regime.

A plot of ξ_{0s} versus l and l/h using the parameters of Table 1 is shown in Fig. 9. The elevation is positive at the spreading ridge and negative at the subduction zone. It is to be noted that for the major plates of the earth, the amplitude is around 1,300 m. For any given plate the regional slope, $\bar{i}_s$, of this surface in the direction from the spreading ridge toward the subduction zone is given by $\bar{i}_s = 2\xi_{0s}/l$.

As an additional example we consider the case for which the lithospheric plate is motionless, changing the first boundary condition to $v_x = 0$, $z = 0$. The solution for ψ is

$$\psi = -\frac{g\sigma \sin kx}{\rho_0 \nu k^3}\left[1 - \cosh kz + \frac{L_1(kz\cosh kz - \sinh kz) - M_1 kz \sinh kz}{k^2h^2 - \sinh^2 kh}\right] \tag{44}$$

where

$$L_1 = \sinh kh \cosh kh - kh \cosh kh - \sinh kh + kh,$$
$$M_1 = \sinh^2 kh - kh \sinh kh \tag{45}$$

and the solution for τ_{zx0} is

$$\tau_{zx0} = \frac{g\sigma \sin kx}{k} \frac{\sinh^2 kh + k^2h^2 - 2kh \sinh kh}{\sinh^2 kh - k^2h^2} \tag{46}$$

which reduces to Eq. (7) for η large.

Horizontal lithospheric density change effects

Hales (1969), Jacoby (1970, 1978), Lister (1975), Hager (1978), and Hager and O'Connell (1981) as well as others have considered a driving related to lithospheric plate gravitational sliding or density change effects, a ridge push force. In particular, Hager and O'Connell's concern was with the density contrasts which result from cooling and thickening of the upper thermal boundary layer, or lithosphere, as it moves away from the spreading ridge. They used the observed plate velocities to calculate the shear stresses through a numerical computational procedure. It seemed instructive to rephrase their problem in the same terms as the solutions of the preceding two sections and to determine the relative importance of the lithospheric, longitudinal density changes vis-a-vis the mantle density gradient.

They chose to approximate the increase in thickness of lithosphere of essentially constant density by a lithosphere of constant thickness and corresponding increase in density. Following their model, as shown in Fig. 10, the plate force balance for an incremental length, Δx, will consist of the difference in the depth integrated forces normal to the two vertical faces of the plates and the tangential mantle drag force. For the linear approximation the integrated normal to the faces will be the integrated pressures, or

$$\int_{-d}^{0} \rho_0 g z dz - \int_{-d+\xi_s}^{0} \left(\rho_0 + \frac{\partial \rho}{\partial x}\Delta x\right) g z dz \tag{47}$$

which gives for the force balance, to first order terms,

$$\rho_0 g i_s d - \tfrac{1}{2} g \lambda d^2 - f_{zx} = 0. \tag{48}$$

For comparison with the linear approximation solution of Eq. (4), the stress boundary condition at the upper surface of the mantle convection cell will now be

$$\tau_{zx} = \rho_0 \nu \frac{\partial v_x}{\partial z} = -f_{zx} = -\rho_0 g i_s d + \frac{1}{2} g \lambda d^2. \tag{49}$$

Following the same solution procedures as before, we obtain

$$v_x = \frac{g\lambda d^2 h^2}{2\rho_0 \nu(4h+6d)}(1-4n+3n^2),\ i_s = \frac{\lambda d}{\rho}\frac{4h+3d}{4h+6d}. \tag{50}$$

The comparison for the plate velocities in the two cases is

$$v_{x0} = \frac{1}{2}\frac{g\lambda d^2 h^2}{\rho_0 \nu(4h+6d)} \tag{51}$$

and

$$v_{x0} = \frac{1}{48}\frac{g\lambda h^3}{\rho_0 \nu} \tag{52}$$

from Eqs. (50) and (4). The value for λ in the two cases will be about the same; Hager and O'Connell (1981) chose a value of $\lambda = 0.0665/l$ for extended plate lengths and from Table 1 we have used a value of $\lambda = 2\sigma/l = 0.04/l$. For values of $d = 100$ km and $h = 600$ km, the ratio between the two v_{x0} values will be $0.6/4.5 = 13\%$. In other words, the lithospheric density changes are a minor contribution to the plate motions as contrasted with the presumed upper mantle density contrast from spreading ridge to subduction zone. This is not an unexpected result as the lithospheric driving force is active over a depth interval of $d = 100$ km as contrasted with the upper mantle driving force which is active over a depth interval of $h = 600$ km.

Hager and O'Connell (1981) also considered the condition for which there is a finite viscosity, ν_1, for the lithosphere with the same lithospheric driving force as discussed in the previous paragraphs. With reference to the geometry of Fig. 11 and Eqs. (1) and (3), the defining equation for plate motion in the linear approximation is

$$\rho_0 \nu_1 \frac{d^2 v_{x1}}{dz^2} = -\rho_0 g i_s + g\lambda z \tag{53}$$

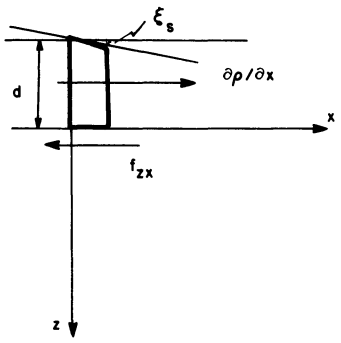

Fig. 10. Geometry for lithospheric density changes as driving force for plate motion and upper mantle convection

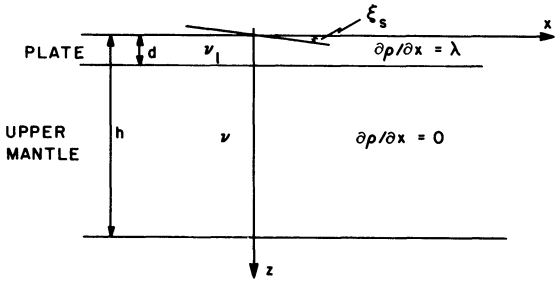

Fig. 11. Geometry for plate and upper mantle convection with lithospheric driving force

and that for the upper mantle is

$$\rho_0 \nu \frac{d^2 v_x}{dz^2} = -\rho_0 g i_s + g\lambda d. \tag{54}$$

Corresponding to the solution of Eq. (4), the boundary conditions are $\tau_{zx1} = 0$, $z = 0$; $\tau_{zx1} = \tau_{zx}$, $v_{x1} = v_x$, $z = d$; $v_x = 0$, $z = h$ and the continuity condition is the same as before. The solution for v_{x10} is

$$v_{x10} = \frac{1}{48}\frac{g\lambda h^3}{\rho_0 \nu} F(\beta, d, h) \tag{55}$$

where $F(\beta, d, h)$ is given as

$$F(\beta, d, h) = \frac{6d^2(h-d)^4 + \beta d^3(h-d)(16h^2 - 17dh + 7d^2) + \beta^2 d^6}{h^3(h^3 - d^3 + \beta d^3)} \tag{56}$$

and where β is the ratio of the two viscosities, defined as $\beta = \nu/\nu_1$. For a rigid plate, $\beta = 0$ and for a plate and upper mantle of the same viscosity, $\beta = 1$.

Taking $d = 100$ km and from the geometry of Fig. 11, $h = 700$ km, $F = 0.0663$ at $\beta = 0$ and $F = 0.1004$ at $\beta = 1$. Comparing with results of Eq. (52) where $h = 600$ km, the ratio between the v_{x0} values will be $0.0663\ (7^3/6^3) = 11\%$ for $\beta = 0$ and $0.1004\ (7^3/6^3) = 16\%$ for $\beta = 1$. Again, the lithospheric driving force contribution for plate motion is small compared with that for an upper mantle flow.

Extended upper mantle convection

In the previous derivations the upper mantle convection has been taken to be limited to the depth interval

from $z=0$ to $z=h$ where h is determined from a combination of both an assumed zone of lower viscosity, v, and a limited extent of plate associated driving forces at the spreading ridge and subduction zone. It is of interest to examine what effects may be anticipated for an extended zone, h_2, of finite viscosity, v_2, in the lower mantle with the same depth extent, h, for the driving forces.

The one dimensional solution to this problem has been given in the previous section. With reference to Fig. 11, we make the following notational changes, $v_1 = v$, $v = v_2$, $d = h$ and $h = h_2$. From Eqs. (55) and (56) we, then, have

$$v_{x0} = \frac{1}{48} \frac{g\lambda h^3}{\rho_0 v} F(\beta, h, h_2) \tag{57}$$

where $F(\beta, h, h_2)$ is now given by

$$F(\beta, h, h_2) = \frac{6(h_2-h)^4 + \beta h(h_2-h)(16h_2^2 - 17hh_2 + 7h^2) + \beta^2 h^4}{\beta h(h_2^3 - h^3 + \beta h^3)} \tag{58}$$

and where $\beta = v_2/v$. The result is the same as that given by Eq. (5) multiplied by the quantity, F.

The anticipated values of viscosity for the lower mantle are such that β may range from $\beta = 1{,}000$ to $\beta = 10$. For $h = 600$ km, as before, and $h_2 = 1{,}200$ km, for example, $F = 1.0$, 1.3, 2.8 for $\beta = 1{,}000$, 100, 10, respectively. The effect of extended upper mantle convection can be important for small values of β and can lead to an increase in the value of v_{x0} by a factor of two or more.

Horizontal heating effects

Allan et al. (1967) considered upper mantle convection driven by a horizontal temperature gradient imposed at the top of the convection cell. They concluded that modest temperature differences along the upper surface of the cell were sufficient to produce upper mantle velocities of the order of 1 cm yr^{-1}. In the derivation they assumed that the nonadvective, or conductivity, heat transfer terms were dominant over the advective heat transfer terms. It is instructive to extend their derivations using the perturbation procedure of Babcock (1930).

The defining equations are

$$\nabla^4 \psi = \frac{\alpha g}{v} \frac{\partial T}{\partial x} \tag{59}$$

and

$$\kappa \nabla^2 T = \mathbf{v} \cdot \nabla T \tag{60}$$

where the horizontal temperature and density gradients are related by

$$\frac{\partial \rho}{\partial x} = -\alpha \rho_0 \frac{\partial T}{\partial x} \tag{61}$$

and where κ is the thermal diffusivity and α the volume coefficient of expansion. The perturbation solutions take the form

$$T = T_0 + \alpha T_1 + \alpha^2 T_2 + \ldots,$$
$$\psi = \alpha \psi_1 + \alpha^2 \psi_2 + \ldots \tag{62}$$

in terms of the small quantity α. The solutions are given sequentially to the equations

$$\nabla^2 T_0 = 0 \tag{63}$$

for terms in α^0,

$$\alpha \nabla^4 \psi_1 = \frac{\alpha g}{v} \frac{\partial T_0}{\partial x} \tag{64}$$

and

$$\alpha \kappa \nabla^2 T_1 = \alpha \left(-\frac{\partial T_0}{\partial x} \frac{\partial \psi_1}{\partial z} + \frac{\partial T_0}{\partial z} \frac{\partial \psi_1}{\partial x} \right) \tag{65}$$

for terms in α^1, and

$$\alpha^2 \nabla^4 \psi_2 = \frac{\alpha^2 g}{v} \frac{\partial T_1}{\partial x} \tag{66}$$

for terms in α^2.

Following Allan et al. (1967), we take an imposed temperature $T = \theta \cos kx$ at $z = 0$ and $T = 0$ at $z = h$ and the same boundary conditions for ψ as in the solution for Eq. (32). The T_0 solution is simply

$$T_0 = \theta \frac{\sinh k(h-z)}{\sinh kh} \cos kx \tag{67}$$

or for large values of $\eta = kh$

$$T_0 = \theta(1-n) \cos kx \tag{68}$$

where $n = z/h$ is the scaled depth. Sequentially, the solutions for ψ_1, T_1 and ψ_2 are

$$\psi_1 = -\frac{gk\theta h^4}{240v}(3n - 11n^3 + 10n^4 - 2n^5) \sin kx, \tag{69}$$

$$T_1 = \frac{gk^2\theta^2 h^5}{6720vk}(2.6n - 21n^2 + 14n^3 + 38.5n^4 - 58.1n^5 + 28n^6 - 4n^7) + \frac{gk^2\theta^2 h^5}{2016vk}(-4.78n + 6.3n^2 - 11.55n^4 + 13.23n^5 - 5.6n^6 + 2.4n^7) \cos 2kx \tag{70}$$

$$\psi_2 = \frac{g^2 k^3 \theta^2 h^9}{100800 v^2 k}(18.92n - 7.16n^3 - 3.98n^5 + 1.75n^6 - 0.69n^8 + 0.44n^9 - 0.11n^{10} + 0.3n^{11}) \cdot \sin 2kx \tag{71}$$

The value for v_{x0} will, then, be

$$v_{x0} = \frac{\alpha g k \theta h^3}{80v} \sin kx - \frac{\alpha^2 g^2 k^3 \theta^2 h^8}{5328 v^2 \kappa} \sin 2kx + \ldots. \tag{72}$$

The ratio, χ, of the two Fourier components is

$$\chi = \frac{\alpha g k^2 \theta h^5}{67 v \kappa}. \tag{73}$$

It is to be noted that the ratio, χ, is in the form of a Rayleigh number. Similar ratios with different numerical coefficient values hold for the succeeding terms. If the first term for v_{x0} is to be dominant, i.e., a single cell convection over the length l, χ should be small. Taking as an extreme example that $\chi=1$, $\theta=0.6\,°C$ for representative value of $\alpha=4\times10^{-5}$, $g=10^3$, $\nu=3\times10^{21}$, and $\kappa=1\times10^{-2}$ in CGS units and for $l=3{,}000$ km and $h=600$ km. The corresponding values for the coefficients in Eq. (72) are, then, 0.01 cm yr^{-1}.

The result is not unexpected. It merely shows that a solution in terms of conductivity heat transfer or perturbations thereto is inadequate to a description of the observed plate motions. The advective heat transfer terms are dominant over the conductivity transfer terms. For an imposed thermal condition at the upper, or lower, surface of the convection cell, the system parameters will lead to degradation of an original, and slower velocity, large aspect ratio cell to smaller scale cells. The results are shown in a more definitive manner from the numerical model results of McKenzie et al. (1974) for the mantle and of Beardsley and Festa (1972) for a similar geophysical fluid dynamic problem.

Adjoining plate motions and asymmetric spreading

There is a corollary to the relation of Eq. (22) that v_{x0} varies as $(b'_1+b'_2)/(b_1+b_2)l$. Consider two adjoining plates with a significant difference in their longitudinal extents, l. As discussed by Morgan (1971) for a different hypothesized plate driving force, the ridge forming basalts would rise passively to fill the void created as the plate are pulled apart. It would be anticipated that plate accretion would occur symmetrically for both plates under such passive conditions whether the plate velocities, v_1 and v_2, with respect to the upper mantle convection cell are the same or are different and that the magnetic patterns would retain a corresponding symmetry, as indeed is the general case. As shown in Fig. 12, the spreading rates with respect to the spreading ridge will be equal and will be given by $(v_1+v_2)/2$. In order for their velocities to be v_1 and v_2 with respect to the upper mantle convection cells, a necessary implication is that the spreading ridge, itself, must move with a velocity $(v_1-v_2)/2$ in the direction of the smaller plate. If there is no change in the location of the subduction zone relative to the spreading ridge, there will be a tendency for the smaller plate to become smaller and eventually disappear and for the larger plate to become larger.

There is a further corollary to the above paragraph, which relates to asymmetric seafloor spreading. Hayes (1976) argues that if one accepts the basic premise of Morgan (1971) that the minimum strength of the lithosphere is determined along the line of maximum temperatures within a narrow injection zone, then it follows that an observation of asymmetric growth requires the locus of accretion to be displaced from the median position by some process which provides a lateral asymmetric temperature profile. From Fig. 12 it can be seen that the projected migrating spreading ridge will provide such a temperature asymmetry with the temperature on the larger plate side of the injection zone being higher than that on the smaller plate side. It

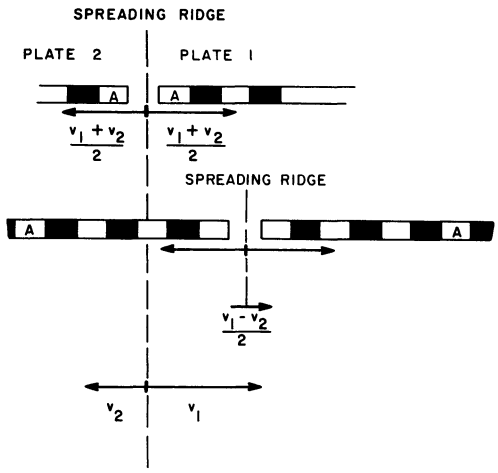

Fig. 12. Schematic representation of spreading and velocity relations for a smaller plate (1) adjacent to a larger plate (2)

would, then, be anticipated that with respect to the spreading ridge, itself, there would be a faster spreading rate on the smaller plate side than on the larger plate side. Further, it would be anticipated that the heat flow would also show a corresponding asymmetry with higher heat flows near the spreading ridge on the larger plate side than on the smaller plate side.

This corollary can be tested by examining the geophysical measurements across a spreading ridge bounded by a plate of smaller l or larger $(b'_1+b'_2)/(b_1+b_2)$ values on one side as compared with a plate of larger l or smaller $(b'_1+b'_2)/(b_1+b_2)$ values on the other side. Weissel and Hayes (1971) and Hayes (1976) observed asymmetric spreading rates across the Southeast Indian ridge of up to 30% over periods of 30 m.y. with the Indian plate of smaller l and larger $(b'_1+b'_2)/(b_1+b_2)$ values spreading at a faster rate as compared with the Antarctic plate. Rea (1978, 1981) has summarized various investigations for the East Pacific rise bounded to the east by the Nazca plate of smaller l value and to the west by the Pacific plate. The findings are that (1) the east flank of the rise has been spreading at a rate of 9.2 cm yr^{-1} as compared with 7.0 cm yr^{-1} for the west flank over the past 2.4 m.y., (2) there have been a series of spreading ridge offsets to the east of 10–15 km occurring over periods of 0.5 m.y. or less, and (3) the average heat flows within 300 km of the ridge axis are 2.5 ± 1.8 μcal cm^{-2} s^{-1} on the west flank as compared with 1.7 ± 0.8 μcal cm^{-2} s^{-1} on the east flank. All three findings are in accordance with the formulation given in the previous paragraph. These two regions were selected because of the definitive investigations for each. It is possible that other regions may not show the same dependency.

Isostasy in a dynamic system

Introduction

The consideration of isostasy, in general, and gravity anomalies, in particular, for an earth system consisting of convective motion in the upper mantle requires additional attention beyond the concepts associated with a static earth.

The reference surface at depth for lithospheric isostatic equilibrium is no longer a horizontal, or equipotential, surface normal to the gravity vector, **g**, but rather a surface for which the normal stress is constant. For upper mantle convection this is the surface, ξ_s, discussed in the previous sections. Consideration, then, of ocean floor relief changes related to cooling of a lithospheric plate in isostatic balance must be made with reference to the surface, ξ_s, rather than to the horizontal. This important condition was stated by Turcotte and Oxburgh (1972) and Schubert and Turcotte (1972).

For calculations of the gravity anomalies related to the elevation changes in the upper surface, ξ_s, and the longitudinal density changes within the convecting layer, consideration must also be given to the shape of the lower surface, ξ_b, as well. If there is no motion in the lower mantle, then the normal stress must be constant along the surface, ξ_b. Otherwise, there would be a longitudinal stress difference which would produce motion in the lower mantle. This normal stress condition at the lower boundary is the counterpart of the normal stress condition at the upper surface. Although it does not affect the motion in the upper mantle, it is necessary for the definition of the condition of the lower mantle. This important condition was brought forward by De Bremaecker (1976). McKenzie (1977) objected to the De Bremaecker formulation in that it added a third and overdetermined boundary condition for the system; the McKenzie objection is valid only under the assumption that the lower surface of the upper mantle convection is constrained to be horizontal.

Gravity anomalies

For the linear approximation of the previous sections and under the assumption of no motion in the lower mantle, the lower surface, ξ_b, of the upper mantle convection can be determined. From Eqs. (2) and (3), we have at $z=\xi_b$.

$$\frac{\partial p}{\partial x}=g\lambda h-\rho_0 g i_s+\rho_0 g i_b=0 \tag{74}$$

or, using the relation between i_s and λ of Eq. (4)

$$i_b=-\frac{5}{8}\frac{\lambda h}{\rho_0}. \tag{75}$$

The slope of the lower surface is in the opposite direction to that of the upper surface.

The gravity anomalies related to the longitudinal density variations within the upper mantle convecting layer and the distortions of the upper and lower surfaces of the layer can be determined from the usual gravity anomaly integral. To first order terms in ξ_s, ξ_b and λ, we have for the convecting layer gravity anomaly, g',

$$g'=\gamma\int_{V_0}\frac{\rho' z_1}{r^{3/2}}dV_0+\gamma\rho_0\int_{V'}\frac{z_1}{r^{3/2}}dV' \tag{76}$$

where V_0 is the undistorted volume of the convecting layer, V' the distortion volumes at the upper and lower surfaces, ρ' the longitudinal density anomaly, γ the gravitational constant, and where $r^2=(x_1-x)^2+y_1^2+z_1^2$, as shown in Fig. 13. For the first integral we have

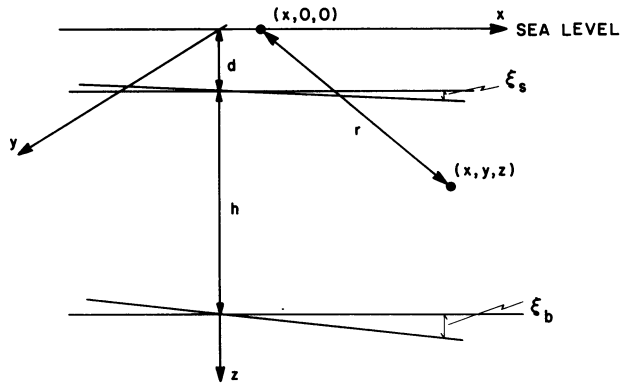

Fig. 13. Geometry for gravity anomaly calculations

$$g'_\lambda=2\gamma\int_d^{h+d}z_1dz_1\int_{-\infty}^{\infty}\frac{\lambda x_1}{(x_1-x)^2+z_1^2}dx_1=2\pi\gamma\lambda hx \tag{77}$$

and for the portion of the second integral related to the upper surface, ξ_s,

$$g'_{\xi_s}=-2\gamma\rho_0\int_{-\infty}^{\infty}\frac{d}{(x_1-x)^2+d^2}dx_1\int_d^{d+i_s x_1}dz_1$$
$$=-2\pi\gamma\rho_0 i_s x \tag{78}$$

and correspondingly

$$g'_{\xi_b}=2\pi\gamma\rho_0 i_b x \tag{79}$$

for the portion of the second integral related to the lower surface ξ_b. From Eqs. (4) and (75), the gravity anomaly gradient is given by

$$\frac{\partial g'}{\partial x}=2\pi\gamma(\lambda h-\rho_0 i_s+\rho_0 i_b)=0. \tag{80}$$

In other words, in the central regime there are no gravity anomalies related to the upper mantle convection itself. This conclusion stems directly from the condition (75). Were this condition relaxed and a horizontal surface taken for the lower surface of the convecting layer, there would be a substantial gravity anomaly gradient given by $\partial g'/\partial x=5\pi\gamma\lambda h/4$.

For the two dimensional approximation of the previous section, the lower surface, $\xi_b=\xi_{0b}\cos kx$, may be determined in the same manner as given by relations (39) through (42), from which we obtain

$$\xi_{0b}=\frac{\sigma}{\rho_0 k}Q(\eta) \tag{81}$$

where

$$Q(\eta)=\frac{2\cosh\eta-2\cosh^2\eta+\eta\sinh\eta}{\eta-\sinh\eta\cosh\eta}. \tag{82}$$

The convecting layer gravity anomalies may also be determined in the same manner as relations (76) through (79), from which we obtain

$$g'=\frac{2\pi\gamma\sigma}{k}[P(\eta)+Q(\eta)e^{-\eta}-(1-e^{-\eta})]e^{-kd}\cos kx \tag{83}$$

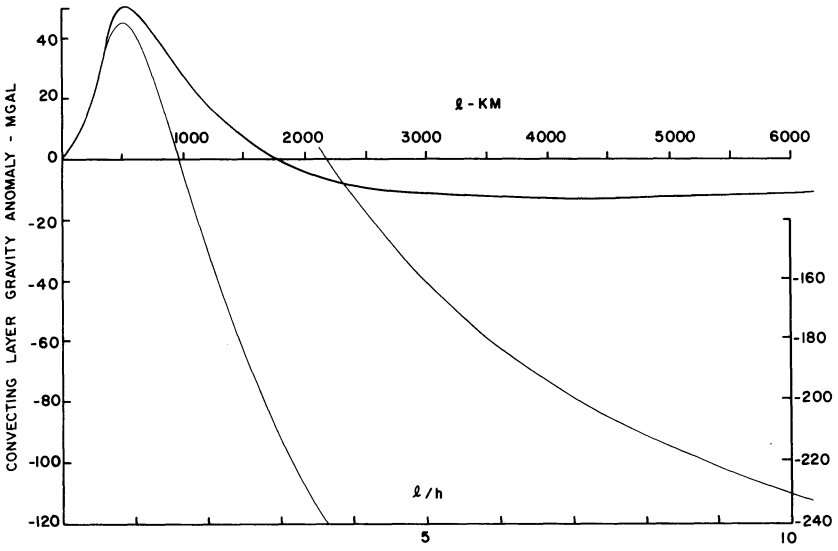

Fig. 14. Graph of amplitude of convecting layer gravity anomaly in mgal versus longitudinal extent in km and aspect ratio. Heavy curve for isostatic condition at lower boundary. Light curve for lower surface of upper mantle convection horizontal. Scale at right applies to second portion of dashed curve

where in the integral (77), λx_1 is replaced by $-\sigma \cos kx$ and where in the integral (78), the limit $d+i_s x_1$ is replaced by $d+\xi_{0s}\cos kx$. The first two terms in the brackets represent the gravity anomaly effects related to the elevation changes at the upper and lower surfaces of the upper mantle convection cell, and the third term in the brackets represents the gravity anomaly effect related to the density changes along the cell.

Following McKenzie (1968), the same relation for the convection cell gravity anomaly may also be derived from Poisson's equation

$$\begin{aligned} \nabla^2 U &= 4\pi\gamma\rho, \quad \text{inside layer,} \\ &= 0, \quad \text{outside layer.} \end{aligned} \tag{84}$$

Substituting $U=U_0+U'=U_0+\theta(z)\cos kx$ and $\rho=\rho_0+\rho'=\rho_0-\sigma\cos kx$ into Eqs. (84), solutions are obtained for U_0 and U' under the boundary conditions that U and ∇U are continuous at the upper and lower surfaces of the cell. To first order terms in ξ_{0s}, ξ_{0b} and σ, the result for $g'=-\partial U/\partial z$ at sea level is the same as that given by Eq. (83).

Figure 14 is a plot of the amplitude, g'_0, for the gravity anomaly of Eq. (83) versus plate length, l, and aspect ratio, l/h, using the parameters of Table 1. For g'_0 positive, the upper mantle convection cell gravity anomaly will be positive over the spreading ridge and negative over the subduction zone. From Fig. 14 it is seen that for most plates g'_0 is negative with a value of around -10 mgal. The density gradient effect is dominant over the surface distortion effects, and the gravity anomaly related to the convection cell, only, is predicted to be negative over the spreading ridge and positive over the subduction zone. It is important to note that these calculations do not include the gravity anomaly effects related to the plate, particularly those that might be anticipated at both the spreading ridge and subduction zone[1].

Also included on Fig. 14 is a plot of the amplitude of the gravity anomaly that would be expected if the lower boundary of the upper mantle convection cell were horizontal rather than determined by a condition of no motion in the lower mantle. The resultant gravity anomalies would be very large with magnitudes of around -200 mgal and easily observable. Anomalies of this magnitude are not found and support the notion that any motion in the lower mantle is probably small in comparison with the upper mantle motion.

The gravity anomalies of Eq. (83) and Fig. 14 relate only to the upper mantle convection cell. They do not have any obvious or direct correlation with the global gravity anomaly pattern of, say, Williamson and Gaposchkin (1973). The association of broad positive anomalies with the subduction zones has been discussed by a number of investigators including Minear and Toksöz (1970), Oxburgh and Turcotte (1970), Griggs (1972), Watts and Talwani (1975), McAdoo (1981) and Chapman and Talwani (1982) using a variety of regional compensation forms for the plate and upper mantle. Chase and McNutt (1982) have shown that only a small part of the geoid anomaly pattern can be explained by the effects of compensated continental and oceanic topography. We suggest that a substantial portion of the remaining gravity anomalies are related to time dependent variations in the upper mantle convective cell properties and lithospheric plate forces which will result in unbalanced but time dependent vertical stresses. In other words, the global gravity anomaly pattern is time dependent with time scales related to the reaction time of the lithosphere to unbalanced vertical stresses, as exemplified by the glacial rebound following the melting of the Fennoscandia and Laurentide ice sheets. That such vertical intraplate movements do occur is shown by the investigation of Officer and Drake (1982) in which rates of uplift and subsidence of 0.1–0.5 cm yr^{-1} were determined along a 3,000 km extent of the East Coast continental margin from Nova Scotia to Florida over the past 18,000 yr.

Ocean floor relief

The variations in ocean floor relief, $D(t)$, away from a spreading ridge as a function of age, t, may be represented by a relation of the form

1 Much of what has been given here is covered in greater detail and generality in a recent paper by Parsons and Daly (1983)

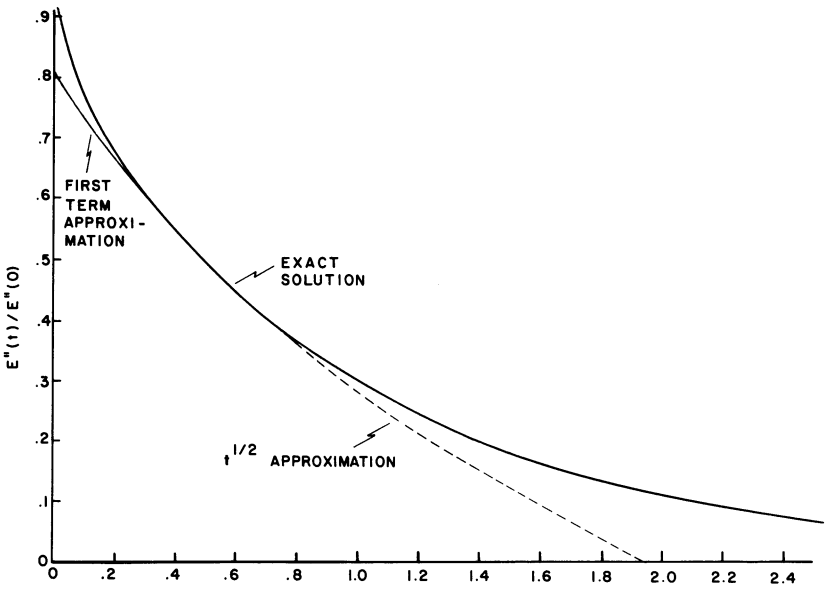

Fig. 15. Graph of $E''(t)/E''(0)$ versus τ from Eqs. (87), *heavy curve*; (88), *light dashed curve* and *heavy curve*; and (89), *light curve* and *heavy curve*

$$D(t)=D'(t)+D''(t) \tag{85}$$

where $D'(t)$ is the depth variation related to the change in elevation of the reference upper mantle convection cell, ξ_s, on which the normal stress is constant and $D''(t)$ is the depth variation related to cooling of the lithospheric plate.

The change in elevation of the upper surface of the convection cell is given by relations (41) and (42), and a plot of its amplitude as a function of plate longitudinal extent using the parameters of Table 1 has been given in Fig. 9. The regional slope of this surface will be $-2\xi_{0s}/l$. As contrasted with the depth changes related to cooling effects, the elevation changes related to the upper mantle convection cell are distance rather than time dependent. However, it is convenient for comparison purposes to cast D' in terms of t rather than x. We may, then, represent $D'(t)$ by

$$D'(t)=D_0+\frac{2\zeta_{0s}}{l}x=D_0+\frac{2\zeta_{0s}v\cos\theta}{l}t \tag{86}$$

where $\zeta_{0s}=-\zeta_{0s}$ and D_0 is a reference base level. The quantity, $v\cos\theta$, is a velocity parameter determined from the relation $dx/dt=v\cos\theta$ where x is the distance from the observation location to the present spreading ridge in the direction of l, t the age at the observation location, and θ the angle between the plate velocity, **v**, and **l**.

At the outset it is instructive to ascertain what order of magnitude the regional slope may have. For a nominal longitudinal extent of a plate of $l=6{,}000$ km and a value of $\zeta_{0s}=1{,}300$ km from Fig. 9, the slope will be 430 m/1,000 km. It is to be noted from Fig. 13 of Parsons and Sclater (1977) that this is, indeed, the same order as the depth changes in the North Pacific and North Atlantic for ages greater than $t=70$ m.y. It would appear that ocean depth changes for $t<70$ m.y. are dominated by the plate cooling effects and that the depth changes for $t>70$ m.y. are dominated by the elevation changes of the upper surface of the mantle convection cell.

The plate cooling model of Sclater and Francheteau (1970) and Parsons and Sclater (1977) is used for the representation of $D''(t)$, from which we have

$$-D''(t)=E''(t)=\frac{4\alpha\rho_0 d T_1}{(\rho_0-\rho_w)\pi^2}\sum_{m=0}^{M}\frac{1}{(2m+1)^2}e^{-(2m+1)^2\frac{\pi^2\kappa t}{d^2}} \tag{87}$$

where ρ_0 is the plate density, ρ_w the seawater density, d the plate thickness, T_1 the temperature along the ridge axis at $t=0$ and along the base of the lithospheric plate, κ the thermal diffusivity, and α the thermal coefficient of expansion and where the summation is taken over a finite number of terms, M, for the rapidly convergent series. For t small, the original expression of Parsons and Sclater (1977) reduces to

$$\frac{E''(t)}{E''(0)}=1-\frac{4}{\pi^{3/2}}\tau^{1/2} \tag{88}$$

and for t large, to

$$\frac{E''(t)}{E''(0)}=\frac{8}{\pi^2}e^{-\tau} \tag{89}$$

where $E''(0)=\alpha\rho_0 d T_1/2(\rho_0-\rho_w)$ and $\tau=\pi^2\kappa t/d^2$. It is instructive to examine over what ranges of τ the two approximations are valid. This is given in Fig. 15. It is seen that the first term approximation, Eq. (89), is valid for $\tau>0.2$. From our final results this corresponds to $t>6$ m.y.

We have followed the same general data analysis procedure as Parsons and Sclater (1977) but with the formulation of Eq. (85) and have used the depth variations for the North Pacific and North Atlantic given in their Fig. 13. We look for a best fit to an equation of the form

$$D(t)=A+at-B\sum_{m=0}^{M}\frac{1}{(2m+1)^2}e^{-(2m+1)^2 bt}. \tag{90}$$

By successive approximations, initial values for A and a were first determined from the linear slope of the $D(t)$ values for $t>70$ m.y. separately for the North Pacific and North Atlantic data. Then, initial values for B and b were determined from a semilogarithmic plot of $A+at-D(t)$ versus t jointly for the two sets of data. Next, the A and a values were corrected for the slope given by the B and b term for $t>70$ m.y. And, finally, new values for B and b were determined from the corrected semilogarithmic plot. For the North Pacific the final result is given by

$$D(t)=5{,}300+5.11t-2{,}600 \cdot \sum_{m=0}^{M} \frac{1}{(2m+1)^2} e^{-\frac{(2m+1)^2 t}{29.8}} \tag{91}$$

and for the North Atlantic by

$$D(t)=5{,}300+4.71t-2{,}600 \cdot \sum_{m=0}^{M} \frac{1}{(2m+1)^2} e^{-\frac{(2m+1)^2 t}{29.8}}. \tag{92}$$

The resultant fits to the data are shown in Figs. 16 and 17. The heavy curves on the figures are from Eqs. (91) and (92) and the light lines from the first two terms of these expressions, or the upper mantle elevation change. It is also to be noted that the reference depths, A, come out to be the same for the North Pacific and North Atlantic, as might be expected.

We may also investigate the variation in heat flow, $q(t)$, as a function of age. From McKenzie (1967) and Parsons and Sclater (1977), we have

$$q(t)=\frac{k_p T_1}{d}\left[1+2\sum_{n=1}^{N} e^{-n^2\frac{\pi^2\kappa t}{d^2}}\right] \tag{93}$$

where k_p is the thermal conductivity and where the summation is taken over a finite number of terms, N, for the slowly convergent series, valid except near $t=0$. For t small, the original expressions of Parsons and Sclater (1977) reduce to

$$\frac{q(t)}{q(\infty)}=\frac{\pi^{1/2}}{\tau^{1/2}} \tag{94}$$

and for t large, to

$$\frac{q(t)}{q(\infty)}=1+2e^{-\tau} \tag{95}$$

where $q(\infty)=k_p T_1/d$. Figure 18 is a plot of these three expressions versus τ. It is seen that the first term approximation, Eq. (95), is valid for $\tau>0.8$. From our final results this corresponds to $t>24$ m.y.

The heat flow data given in Table 1 of Sclater et al. (1980) was used for comparison purposes. The $q(\infty)$ value was determined from the heat flow data for $t>100$ m.y. with the small correction given by Eq. (95) and the value of τ from Eqs. (91) and (92). The final result is given by

$$q(t)=1.17\left[1+2\sum_{n=1}^{N} e^{-\frac{n^2 t}{29.8}}\right]. \tag{96}$$

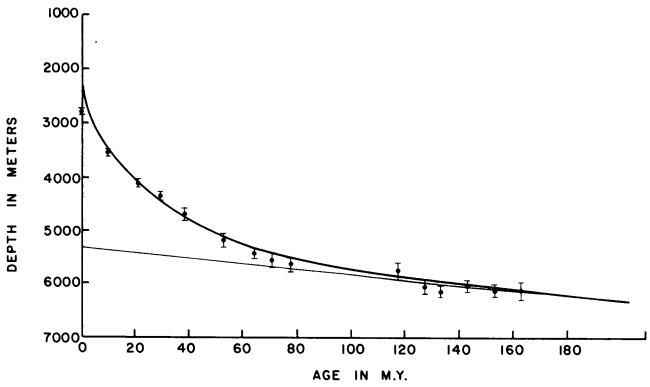

Fig. 16. Plot of mean depth measurements and standard deviation versus age for the North Pacific. Data from Parsons and Sclater (1977). *Heavy curve*, Eq. (91) and *light line*, the first two terms of the equation

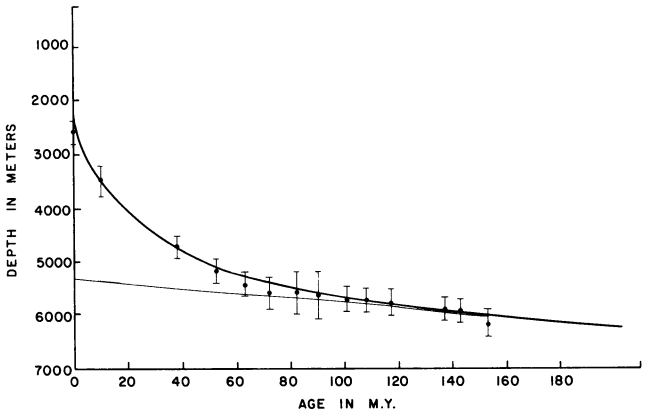

Fig. 17. Plot of mean depth measurements and standard deviation versus age for the North Atlantic. Data from Parsons and Sclater (1977). *Heavy curve*, Eq. (92) and *light line*, the first two terms of the equation

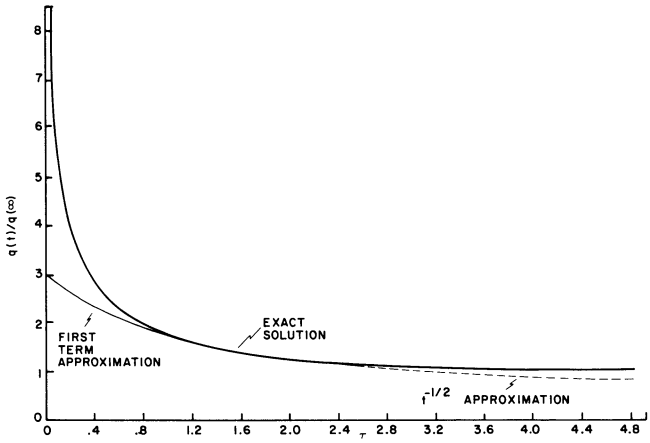

Fig. 18. Graph of $q(t)/q(\infty)$ versus τ from Eqs. (93), *heavy curve*; (94), *light dashed curve* and *heavy curve*; and (95), *light curve* and *heavy curve*

The resultant fit to the data is shown in Fig. 19. As discussed by Sclater et al. (1980) as well as others, the departure for $t<50$ m.y. may be due to hydrothermal circulation effects.

Further, we have followed the same procedure as

Parsons and Sclater (1977) for determining values of d, T_1 and α. We use their given values of $\rho_0 = 3.33$, $\rho_w = 1.0$, $c_p = 0.28$, and $k_p = 7.5 \times 10^{-3}$ all in CGS units from which $\kappa = k_p/\rho_0 c_p$ is also given. Successively, d is determined from the b value, T_1 from the $q(\infty)$ value and α from the B value. We obtain $d = 86$ km, $T_1 = 1{,}350\,^\circ$C and $\alpha = 3.85 \times 10^{-5}$. All are reasonable values. The principal difference between our analysis and theirs, which does not include the mantle elevation changes, is in the time constant for the exponential. They obtained a value of 62.8 m.y.$^{-1}$ as compared with our value of 29.8 m.y.$^{-1}$. This, in turn, leads to the differences in their values of $d = 125$ km and $q(\infty) = 0.8$ μcal cm^{-2} s^{-1} as compared with our values of 86 km and 1.17 μcal cm^{-2} s^{-1}. In passing, we also note that their result of $q(t) = 11.3 t^{-1/2}$ for the approximation (94) is the same with our values.

Finally, we have calculated a value for the parameter, v, from the relation, $b = 2\zeta_{0s} v \cos\theta / l$, of Eq. (86). It is appreciated that the value of $\zeta_{0s} = 1{,}300$ m from Fig. 9 applies only to the simplified derivations of the previous sections and is not directly applicable to actual lithospheric plates of more complex geometry and with varying lengths of bounding spreading ridge and subduction zone. Nevertheless, we do anticipate that, as with the plate velocities of Fig. 8, the values determined for v will be of the same order of magnitude as actually occur. The b values for the North Pacific and North Atlantic are 5.11 ± 0.78 and 4.71 ± 0.43 m m.y.$^{-1}$. Taking nominal plate extents, l, of 13,000 km for the North Pacific and 8,000 km for the North Atlantic and a value of $\theta = 60°$ for $t > 70$ m.y. for the North Pacific, the time extent over which the b parameter was calculated, v is 5.1 and 1.5 cm yr^{-1}, respectively. These values are in reasonable agreement with the present spreading rates but are somewhat too low for the expected time average values for v.

There is a corollary to the ocean floor relief relation

$$D(t) = D_0 + \frac{2\zeta_{0s} v \cos\theta}{l} t - \frac{4\alpha\rho_0 d T_1}{(\rho_0 - \rho_w)^2} \cdot \sum_{m=0}^{M} \frac{1}{(2m+1)^2} e^{-(2m+1)^2 \frac{\pi^2 \kappa t}{d^2}} \tag{97}$$

which provides an interesting test as to its general validity. The upper mantle elevation term varies inversely as a function of l and directly as a function of v. In particular, for two plates adjacent to a spreading ridge for which there is a significant difference in the longitudinal extents, l, it is anticipated that the ocean floor relief plotted as a function of t, or x, will show greater depths on the smaller plate than on the larger plate at the same values of t with a linear variation in the difference as a function of distance away from the spreading ridge. For the examples cited in the following two paragraphs there is also a change in the v value for the two plates of up to 30%. However, the dominant change is in the values for l. We may, then, represent $\Delta D'(t)$ by

$$\Delta D'(t) = \frac{2\zeta_{0s}(l_2 - l_1)}{l_1 l_2} x = \frac{2\zeta_{0s}(l_2 - l_1) v}{l_1 l_2} t \tag{98}$$

where $\theta = 0$.

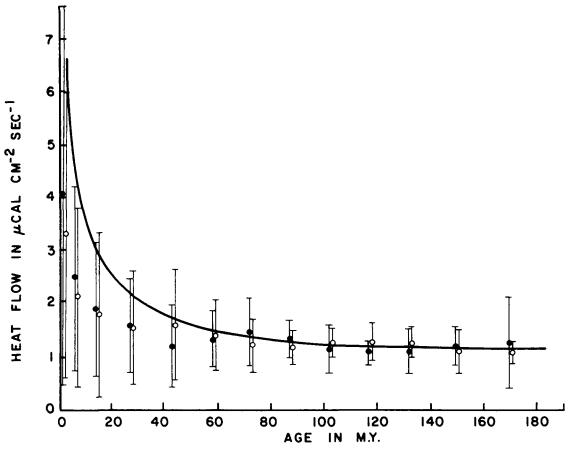

Fig. 19. Plot of mean heat flow measurements and standard deviation versus age for the North Pacific and North Atlantic. Data from Sclater et al. (1980); ● - North Pacific and ○ - North Atlantic. Curve from Eq. (96)

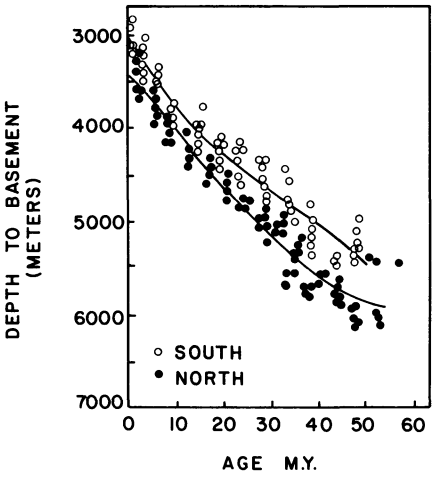

Fig. 20. Plot of depth to basement versus age across the Southeast Indian ridge from Hayes (1976). Indian plate to the north and Antarctic plate to the south

Hayes (1976) discusses the ocean floor relief variations across the Southeast Indian ridge, bounded to the north by the Indian plate and to the south by the Antarctic plate. Figure 20 is his plot of basement depths as a function of age. It shows a gradual increase in the relief difference. At 40 m.y., corresponding to $x = 1{,}100$ km, the relief difference is 500 m. Using nominal plate lengths of $l = 4{,}200$ km for the Indian plate and 8,000 km for the Antarctic plate and $\zeta_{0s} = 1{,}300$ m, $\Delta D'(t) = 300$ m at 40 m.y. from Eq. (98). The calculated value is of the same order of magnitude as that observed with the relief difference in the same direction, greater depths on the smaller plate. The conjecture by Weissel and Hayes (1974) that this relief difference is related to upper mantle causes would appear to be correct.

A similar situation exists for the East Pacific rise, bounded to the east by the Nazca plate and to the west by the Pacific plate. Figure 21 from Mammerickx et al. (1975) is a plot of the ocean floor relief as a function of

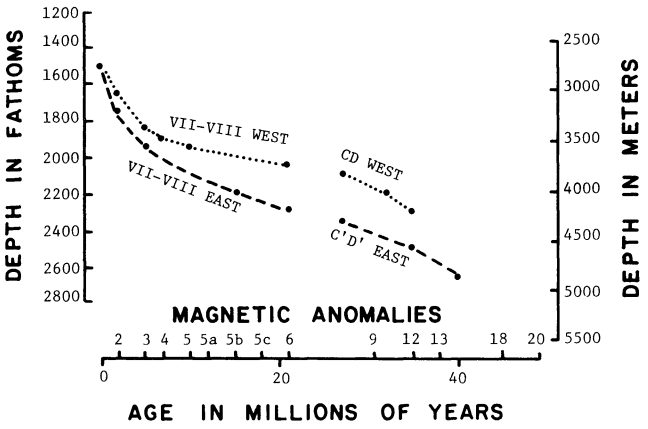

Fig. 21. Plot of ocean floor relief versus age across the East Pacific rise from Mammerickx et al. (1975). Nazca plate to the east and Pacific plate to the west

age for the two adjoining plates. It also shows increased depths on the smaller plate and an approximate linear increase in the relief difference. At 20 m.y., corresponding to $x = 1{,}600$ km, the relief difference is 500 m. Using nominal plate lengths of $l = 3{,}700$ km for the Nazca plate and $l = 10{,}000$ km for the Mid Pacific plate and $\zeta_{0s} = 1{,}300$ m, $\Delta D'(t) = 700$ m at 20 m.y. from Eq. (98). As for the Southeast Indian ridge, the calculated value is of the same order of magnitude as that observed with the relief difference in the same direction.

Summary and discussion

A quantitative description of plate dynamics and related upper mantle effects has been given. The principal driving force for the upper mantle convection is the longitudinal density gradient in the upper mantle between the spreading ridge and the subduction zone. Plate forces, asthenospheric-lithospheric coupling, and lithospheric density changes have also been included in the derivations as well as possible depth variations of viscosity in the upper mantle, and their effects have been assessed.

The derivations have been applied to the various geophysical observables related to plate tectonics. It is found that the derived plate velocities are of the same order as those observed and that the predicted and observed plate velocity variations as a function of plate geometry show the same general dependence. The theoretical formulation provides a mechanism to explain observed spreading ridge migration and asymmetric seafloor spreading effects.

The computed gravity anomalies related to the upper mantle convection are small, being negative over the spreading ridge and positive over the subduction zone. The addition of the predicted upper mantle, reference surface relief to lithospheric plate cooling effects is in agreement with observed ocean floor relief and provides an explanation for the observed relief at ages greater than 70 m.y. The predicted variation in the upper mantle reference surface relief as a function of plate geometry is in agreement with the related observations and provides an explanation for asymmetric variations in ocean floor relief.

A few comments are appropriate concerning continuing investigations by others along lines similar to those given above. Richter and Parsons (1975) as well as others have emphasized that two scales of motion are possible in the upper mantle, one with a large aspect ratio related to the plate dimensions and the other with a small aspect ratio related to Rayleigh-Benard thermal convection. In their formulation the former is associated with the plate motions and is attributed to gravitational forces of the plates themselves without the inclusion of the gravitational forces in the upper mantle, as discussed in this paper. Chapman et al. (1980) and Hewitt et al. (1980) have shown that large aspect ratio upper mantle convection can exist when the upper and lower boundary conditions for the upper mantle are given in terms of a constant heat flux rather than a constant temperature condition. The constant flux condition is also explicit in the derivations of Rattray and Hansen (1962), Hansen and Rattray (1965), Officer (1976) and Festa and Hansen (1976) for gravitational circulation in estuaries; in this case the condition is that of no salt flux at the surface and bottom of the estuary. The principal difference between the expositions given by Chapman et al. (1980) and Hewitt et al. (1980) and that given here is the emphasis, here, on the importance of the longitudinal density gradient between the hotter and less dense spreading ridge column at one end of the convection cell and the cooler and more dense subducted slab column at the other end. It appears to us that their considerations and those given here are headed in the same direction toward an explanation of plate dynamics and the differences may be only a matter of degree in formulation; both lead to a longitudinal density gradient in the upper mantle between the spreading ridge region and the subduction zone. Also, the interesting experimental work of Carrigan (1982) provides a clear demonstration that both scales of motion can exist. The smaller scale, Rayleigh-Benard, thermal convection is confined to the region near the upper surface of the convecting fluid. The larger scale motion consists of two cells, sinking at the lateral walls of the experimental chamber and rising in the central region. Carrigan suggests that the larger scale motion may be related to loss of heat to the sidewalls of the chamber, along the same lines as given here. Further, the detailed theoretical and experimental investigations by Rabinowicz et al. (1980), Froidevaux and Nataf (1981) and Nataf et al. (1981) on the effects of the cooler subducted slab in creating large aspect ratio convection in the subcontinental mantle follow similar precepts to those considered here. The principal difference between their description and that given here is that we have also included the anticipated effects of the hotter spreading ridge column, which effectively defines the longitudinal extent of the upper mantle convection related to the plate motions.

The emphasis in this paper has been on deriving simple analytic solutions for upper mantle, gravitational circulation and associated plate motions and on applying these results to the various geophysical observables related to plate tectonics. We appreciate that in some cases the applications overextend the simple derivations, but we considered that it was appropriate to get at least some notion as to whether they were com-

patible with the observables. We also appreciate that fitting the data to our simple model, such as for the case of oceanic depth variations greater than 70 m.y., does not in itself prove the validity of the model. It is simply data fitting, and there are usually enough undetermined parameters that a good fit can be obtained to various models. For example, Heestand and Crough (1981) explain the oceanic depth variations for ages greater than 80 m.y. and Stein et al. (1977) explain asymmetric sea floor spreading in terms of the hot spot circulation model of Morgan (1972a, 1972b).

We have attempted to point out the relative importance of the possible plate driving forces in a coupled lithosphere-asthenosphere system, viz., upper mantle longitudinal density gradient, lithospheric density changes or ridge push, and negative buoyancy of the subducted slab or slab pull. The importance of each depends in large part on the values chosen for the defining parameters. In particular, as a more realistic viscosity versus depth relation is taken for the lithosphere and asthenosphere, such as that proposed by Anderson (1979), and as proper consideration is given to the thickness variations of the plate itself, such as that proposed by Chapman and Pollack (1977), the formulations given by Hager and O'Connell (1981) and by Richter and McKenzie (1978) for the lithospheric force contributions and that given here for the upper mantle circulation must all be included to arrive at an appropriate representation for the geodynamics of the coupled system.

Acknowledgements. We appreciate and gratefully acknowledge the commentary we have received from T.J. Ahrens, D.L. Anderson, O.L. Anderson, R.L. Carlson, C.R. Carrigan, N. Irvine, W.R. Jacoby, T.H. Jordan, D.P. McKenzie, F.M. Richter, and S. Uyeda in this continuing discussion on how the earth works.

References

Allan, D.W., Thompson, W.B., Weiss, N.O.: Convection in the earth's mantle. In: Mantles of the earth and terrestrial planets. S.K. Runcorn, ed.: pp 507–512. London: Wiley 1967

Anderson, D.L.: The deep structure of continents. J. Geophys. Res. **84**, 7555–7560, 1979

Babcock, R.W.: Thermal convection. Phys. Rev. **35**, 1008–1013, 1930

Backus, G., Park, J., Garbasz, D.: On the relative importance of the driving forces of plate motion. Geophys. J. R. Astron. Soc. **67**, 415–435, 1981

Beardsley, R.C., Festa, J.F.: A numerical model of convection driven by a surface stress and non-uniform horizontal heating. J. Phys. Oceanogr. **2**, 444–455, 1972

Carlson, R.L.: Boundary forces and plate velocities. Geophys. Res. Lett. **9**, 958–961, 1981

Carlson, R.L., Hilde, T.W.C., Uyeda, S.: The driving mechanism of plate tectonics: Relation to age of the lithosphere at trenches. Geophys. Res. Lett. **10**, 297–300, 1983

Carrigan, C.R.: Multiple scale convection in the earth's mantle: A three dimensional study. Science **215**, 965–967, 1982

Cathles, L.M.: The viscosity of the earth's mantle. Princeton: Princeton Univ. Press 1975

Chapman, C.J., Childress, S., Proctor, M.R.E.: Long wavelength thermal convection between nonconducting boundaries. Earth Planet Sci. Lett. **51**, 362–369, 1980

Chapman, D.S., Pollack, H.N.: Regional geotherms and lithospheric thickness. Geology **5**, 265–268, 1977

Chapman, M.E., Talwani, M.: Geoid anomalies over deep sea trenches. Geophys. J. R. Astron. Soc. **68**, 349–369, 1982

Chapple, W.M., Tullis, T.E.: Evaluation of the forces that drive the plates. J. Geophys. Res. **82**, 1967–1984, 1977

Chase, C.G., McNutt, M.K.: The geoid effect of compensated topography and uncompensated ocean trenches. Geophys. Res. Lett. **9**, 29–32, 1982

De Bremaecker, J.-C.: Relief and gravity anomalies over a convecting mantle. Geophys. J. R. Astron. Soc. **45**, 349–356, 1976

Festa, J.F., Hansen, D.V.: A two dimensional numerical model of estuarine circulation: The effects of altering depth and river discharge. Estuarine Coastal Mar. Sci. **4**, 309–323, 1976

Forsyth, D., Uyeda, S.: On the relative importance of the driving forces of plate motion. Geophys. J. R. Astron. Soc. **43**, 163–200, 1975

Froidevaux, C., Nataf, H.C.: Continental drift: What driving mechanism. Geol. Rund. **70**, 166–176, 1981

Gordon, R.G., Cox, A., Harter, C.E.: Absolute motion of an individual plate estimated from its ridge and trench boundaries. Nature **274**, 752–755, 1978

Griggs, D.T.: The sinking lithosphere and the focal mechanism of deep earthquakes. In: The nature of the solid earth. E.C. Robertson, ed.: pp 361–384. New York: McGraw-Hill 1972

Hager, B.H.: Oceanic plate motions driven by lithospheric thickening and subducted slabs. Nature **276**, 156–159, 1978

Hager, B.H., O'Connell, R.J.: A simple global model of plate dynamics and mantle convection. J. Geophys. Res. **86**, 4843–4867, 1981

Hales, A.L.: Gravitational sliding and continental drift. Earth Planet Sci. Lett. **6**, 31–34, 1969

Hansen, D.V., Rattray, M.: Gravitational circulation in straits and estuaries. J. Mar. Res. **23**, 104–122, 1965

Hayes, D.E.: Nature and implications of asymmetric sea floor spreading: Different rates for different plates. Geol. Soc. Am. Bull. **87**, 994–1002, 1976

Heestand, R.L., Crough, S.T.: The effect of hot spots on the oceanic age-depth relation. J. Geophys. Res. **86**, 6107–6114, 1981

Hewitt, J.M., McKenzie, D.P., Weiss, N.O.: Large aspect ratio cells in two dimensional thermal convection. Earth Planet Sci. Lett. **51**, 370–380, 1980

Irvine, T.N.: Density current models of tectonic processes. Carnegie Inst. Wash. Yearb. **78**, 450–461, 1979

Jacoby, W.R.: Instability in the upper mantle and global plate movements. J. Geophys. Res. **75**, 5671–5680, 1970

Jacoby, W.R.: One dimensional modelling of mantle flow. Pure Appl. Geophys. **116**, 1231–1249, 1978

Jordan, T.H.: The continental tectosphere. Rev. Geophys. Space Phys. **13**, 1–12, 1975

Jordan, T.H.: The deep structure of the continents. Sci. Am. **240**, 92–107, 1979

Lister, C.R.B.: Gravitational drive on oceanic plates caused by thermal contraction. Nature **257**, 663–665, 1975

Mammerickx, J., Anderson, R.N., Menard, H.W., Smith, S.M.: Morphology and tectonic evolution of the East-Central Pacific. Geol. Soc. Am. Bull. **86**, 111–118, 1975

McAdoo, D.C.: Geoid anomalies in the vicinity of subduction zones. J. Geophys. Res. **86**, 6073–6090, 1981

McConnell, R.K.: Viscosity of the mantle from relaxation time spectra of isostatic adjustment. J. Geophys. Res. **73**, 7089–7105, 1968

McKenzie, D.P.: The viscosity of the lower mantle. J. Geophys. Res. **71**, 3995–4010, 1966

McKenzie, D.P.: Some remarks on heat flow and gravity anomalies. J. Geophys. Res. **72**, 6261–6273, 1967

McKenzie, D.P.: The influence of the boundary conditions and rotation on convection in the earth's mantle. Geophys. J. R. Astron. Soc. **15**, 457–500, 1968
McKenzie, D.P.: Surface deformation, gravity anomalies and convection. Geophys. J. R. Astron. Soc. **48**, 211–238, 1977
McKenzie, D.P., Roberts, J.M., Weiss, N.O.: Convection in the earth's mantle. Towards a numerical simulation. J. Fluid Mech. **62**, 465–538, 1974
Minear, J.W., Toksöz, M.N.: Thermal regime of a downgoing slab and new global tectonics. J. Geophys. Res. **75**, 1397–1419, 1970
Morgan, W.J.: Convection plumes in the lower mantle. Nature **230**, 42–43, 1971
Morgan, W.J.: Deep mantle convection plumes and plate motions. Am. Assoc. Petrol. Geol. Bull. **56**, 203–213, 1972a
Morgan, W.J.: Plate motions and deep mantle convection. Geol. Soc. Am. Mem. **132**, 7–22, 1972b
Nataf, H.C., Froidevaux, C., Levrat, J.L., Rabinowicz, M.: Laboratory convection experiments: Effects of lateral cooling and generation of instabilities in the horizontal boundary layers. J. Geophys. Res. **86**, 6143–6154, 1981
Officer, C.B.: Physical oceanography of estuaries. New York: Wiley 1976
Officer, C.B., Drake, C.L.: Epeirogenic plate movements. J. Geol. **90**, 139–153, 1982
Oxburgh, E.R., Turcotte, D.L.: Thermal structure of island arcs. Geol. Soc. Am. Bull. **81**, 1665–1688, 1970
Parsons, B., Daly, S.: The relationship between surface topography, gravity anomalies, and temperature structure of convection. J. Geophys. Res. **88**, 1129–1144, 1983
Parsons, B., Sclater, J.G.: An analysis of ocean floor bathymetry and heat flow with age. J. Geophys. Res. **82**, 803–827, 1977
Pekeris, C.L.: Thermal convection in the interior of the earth. Monthly Notices R. Astron. Soc., Geophys. Suppl. **3**, 343–367, 1935
Peltier, W.R., Andrews, J.T.: Glacial isostatic adjustment – I. The forward problem. Geophys. J. R. Astron. Soc. **46**, 605–646, 1976
Rabinowicz, M., Lago, B., Froidevaux, C.: Thermal transfer between the continental asthenosphere and the oceanic lithosphere. Its effect on subcontinental convection. J. Geophys. Res. **85**, 1839–1853, 1980
Rattray, M., Hansen, D.V.: A similarity solution for circulation in an estuary. J. Mar. Res. **20**, 121–133, 1962
Rea, D.K.: Asymmetric seafloor spreading and a nontransform axis offset: The East Pacific rise 20° S survey area. Geol. Soc. Am. Bull. **89**, 836–844, 1978
Rea, D.K.: Tectonics of the Nazca-Pacific divergent plate boundary. Geol. Soc. Am. Mem. **154**, 27–62, 1981
Richter, F.M.: Dynamical models for sea floor spreading. Rev. Geophys. Space Phys. **11**, 223–287, 1973
Richter, F.M.: On the driving mechanism of plate tectonics. Tectonophys. **38**, 61–88, 1977
Richter, F., McKenzie, D.: Simple plate models of mantle convection. J. Geophys. **44**, 441–471, 1978
Richter, F.M., Parsons, B.: On the interaction of two scales of convection in the mantle. J. Geophys. Res. **80**, 2529–2541, 1975
Ringwood, A.E.: Phase transformations and differentiations in subducted lithosphere: Implications for mantle dynamics, basalt petrogenesis and crustal evolution. J. Geol. **90**, 611–643, 1982
Sammis, C.G., Smith, J.C., Schubert, G., Yuen, D.A.: Viscosity depth profile of the earth's mantle: Effects of polymorphic phase transitions. J. Geophys. Res. **82**, 3747–3761, 1977
Schubert, G., Turcotte, D.L.: One dimensional model of shallow mantle convection. J. Geophys. Res. **77**, 945–951, 1972
Sclater, J.G., Francheteau, J.: The implications of terrestrial heat flow observations on current tectonic and geochemical models of the crust and upper mantle of the earth. Geophys. J. R. Astron. Soc. **20**, 509–542, 1970
Sclater, J.G., Jaupart, C., Galson, D.: The heat flow through oceanic and continental crust and the heat loss of the earth. Rev. Geophys. Space Phys. **18**, 269–311, 1980
Sclater, J.G., Parsons, B., Jaupart, C.: Oceans and continents: Similarities and differences in the mechanisms of heat loss. J. Geophys. Res. **86**, 11535–11552, 1981
Stein, S., Melosh, H.J., Minster, J.B.: Ridge migration and asymmetric sea floor spreading. Earth Planet Sci. Lett. **36**, 51–62, 1977
Toksöz, M.N.: The subduction of the lithsosphere. Sci. Am. **233**, 89–98, 1975
Turcotte, D.L., Oxburgh, E.R.: Mantle convection and the new global tectonics. Ann. Rev. Fluid Mech. **4**, 33–68, 1972
Uyeda, S.: The new view of the earth. San Francisco: W.H. Freeman 1978
Watts, A.B., Talwani, M.: Gravity effects of downgoing lithospheric slabs beneath island arcs. Geol. Soc. Am. Bull. **86**, 1–4, 1975
Weissel, J.K., Hayes, D.E.: Asymmetric seafloor spreading south of Australia. Nature **231**, 518–522, 1971
Weissel, J.K., Hayes, D.E.: The Australian-Antarctic discordance: New results and implications. J. Geophys. Res. **79**, 2579–2587, 1974
Williamson, M.R., Gaposchkin, E.M.: Estimate of gravity anomalies. In 1973 Smithsonian standard earth (III), E.M. Gaposchkin, ed.: Smithsonian Astrophysical Observatory, Special Report 353, 193–228, Cambridge, Mass., 1973

Received December 1, 1982; Revised version June 1, 1983
Accepted June 24, 1983